DTU Sustain

# UAS Hydrometry Surveys in Torne River, Sweden

Freja Damgaard Christensen (s215103)

**Supervisors:**
**Peter Bauer-Gottwein**
**Roland Löwe**

**Bachelor Project**
**December, 2024**

# Abstract

Due to more frequent extreme weather events that can e.g. result in flooding of rivers, more cost- and operational efficient methods are needed for hydrometric river monitoring. Additionally, traditional in-situ hydrometry surveys often face limitations for rivers in remote and hard-to-reach areas. Therefore, this project investigates possibilities of using Unmanned Aerial System (UAS) hydrometry surveys and observations from satellite missions instead of traditional in situ measurements to model Water Surface Elevation (WSE). The focus of the project is the Torne River, which is located in Sweden. From the 3rd to the 9th of September 2024, 23 field sites distributed on two areas of interest on the Torne River have been surveyed. UAS-borne Water Penetrating Radar (WPR) have been used to map the river bathymetry, a Real-Time Kinematic (RTK) Global Navigation Satellite System (GNSS) receiver have been used to measure ground truth WSE, and two datasets from Surface Water and Topography (SWOT) satellite mission are available for the survey days. Based on the WPR data and Digital Elevation Model (DEM) data, cross sectional geometry information for each field site is derived. The cross sectional geometry information is used to set up two hydraulic models for each priority area; one using a Steady-State solver and one using the MIKE+ software. The Manning numbers along the river reaches are calibrated against the WSE observations from the SWOT 456 satellite dataset using the SS-solver. The calibration resulted in Manning numbers of 0.023-0.10 $s/m^{1/3}$ for area 1, and 0.03-0.16 $s/m^{1/3}$ for area 2.

The hydraulic models are used to construct rating curves at chainage locations, where observations from the Sentinel-3 satellite mission are obtained within two defined virtual stations (Övertorneå and Pello). These rating curves are used to predict the discharge at a given WSE observed by a Sentinel-3 satellite, and thereby construct a river discharge time series. The discharge predicted at Övertorneå virtual station was found to be closer to the in-situ discharge than the discharge predicted at Pello virtual station. At the Pello virtual station the predicted discharge was generally overestimated, which is likely due to the presence of an overfall in the downstream end of the virtual station.

# Sammenfatning

På grund af hyppigere ekstreme vejrfænomener, som kan resultere i f.eks. oversvømmelser af floder, er der et øget behov for mindre omkostningsfulde og mere driftsvenlige metoder til hydrometrisk overvågning af floder. Traditionelle hydrometriske metoder støder ofte på udfordringer, når det drejer sig om floder i fjerntliggende eller utilgængelige områder. Derfor undersøger dette projekt muligheden for at anvende ubemandede luftfartøjer (UAS) til hydrometriske målinger samt satellitobservationer som erstatning for traditionelle in-situ målinger til modellering af overfladeelevationen i floder (WSE). Projektet fokuserer på Torne Å i Sverige, hvor 23 tværsnit fordelt på to områder er blevet undersøgt mellem den 3. og 9. september 2024. UAS-båret georadar (WPR) blev brugt til at kortlægge flodens batymetri, en Real-Time Kinematic (RTK) Global Navigation Satellite System (GNSS) modtager blev anvendt til at måle WSE, og to datasæt fra Surface Water and Topography (SWOT) satellitmissionen var tilgængelige mellem d. 3.-9. september. Baseret på WPR-data og Digital Elevationsmodel (DEM) data er tværsnitsgeometrien for hver undersøgt lokation blevet bestemt. På baggrund af tværsnitsgeometrien for de 23 lokationer, er to hydrauliske modeller blevet konstrueret for hvert område: én ved hjælp af en Steady-State solver og én ved brug af MIKE+ software. Manning-tal langs flodens blev kalibreret ift. SWOT 456 satellit observationer, hvilket resulterede i Manning-tal på 0,023-0,10 $s/m^{1/3}$ for område 1 og 0,03-0,16 $s/m^{1/3}$ for område 2.

De hydrauliske modeller blev derefter brugt til at konstruere Q-h kurver ved lokationer, hvor målinger fra Sentinel-3 satellitmissionen er blevet observeret indenfor de to definerede virtuelle stationer (Övertorneå og Pello). Q-h kurverne blev brugt til at forudsige vandføringen ved en given WSE observeret af Sentinel-3, og dermed til at konstruere en tidsserie for flodens vandføring. Den beregnede vandføring ved den virtuelle station i Övertorneå viste sig at være tættere på in-situ målingerne end den beregnede vandføring ved den virtuelle station i Pello. Ved Pello-stationen blev den beregnede vandføring generelt overestimeret, hvilket sandsynligvis skyldes tilstedeværelsen af et overfald i den nedstrøms ende af den virtuelle station

# Preface

This bachelor project is written by Freja Damgaard Christensen as a part of a bachelor degree in Environmental Engineering at DTU. The project was carried out during the Fall semester of 2024 and is a 15 ECTS point project. As part of the Unmanned Airborne Water Observing System (UAWOS) project, UAS hydrometry surveys have been conducted along the Torne River. Peter Bauer-Gottwein, professor at the Department of Geosciences and Natural Resource Management at the University of Copenhagen, has been the supervisor of the project.

I would like to thank Peter Bauer-Gottwein for good supervision, inspiration, and guidance throughout the project. I am thankful that I got to participate in the field survey at the Torne River, and I would like to acknowledge and thank everyone who participated in the field survey.

# Contents

Front page image: DJI M300 drone carrying WPR payload and measuring river bathymetry of a survey site in the Torne River. Picture taken by Freja Damgaard Christensen.

# 1 Introduction

Accurate hydraulic models of the Water Surface Elevation (WSE) along river reaches are important as they, among other, are used to manage water resources efficiently, predict flood risks, and safeguard communities [1]. The accuracy of the model predictions depends directly on the quality of the cross-sectional geometry data, and therefore cross-sectional geometry data is important when setting up hydraulic models for rivers [2]. Traditionally, bathymetry surveys have be made with a Real-Time Kinematic (RTK) Global Navigation Satellite System (GNSS) receiver in rivers with shallow water [3]. These surveys are costly, time consuming and often face limitations for rivers in remote and hard-to-reach areas [4]. Therefore, more cost- and operational efficient methods are needed for hydrometric river monitoring [4]. Additionally, recent studies have shown that WSE observations of inland water bodies made by satellites can be used instead of in-situ observations for calibrating hydraulic models [5, 6].

A combination of data from the Surface Water and Topography (SWOT) satellite mission and Unmanned Aerial System (UAS) hydrometry datasets is possibly a better solution for hydrometric river monitoring compared to the traditional in-situ methods. Therefore, the aim of this project is to explore and compare the possibilities of using UAS hydrometry surveys and WSE observations from the SWOT mission instead of traditional in situ measurements to model the WSE along a river reach. Drone-borne Water Penetrating Radar (WPR) surveys has been conducted to map the river bathymetry and thus get accurate cross-sectional geometry data for field sites along the river reach. The UAS hydrometry surveys has been conducted along the Torne River as part of the Unmanned Airborne Water Observing System (UAWOS) project. As severe floodings in the Torne River in northern Sweden have recently been reported (in 2023) [7], the Torne River is the scope of the project.

Lastly, the project aims to demonstrate that the hydraulic models can be used to develop a virtual gauging station on the Torne River. At the virtual stations the goal is to develop an observation system that can predict discharge based on WSE observations from satellites. In this project, the focus is on WSE observations from the Sentinel-3 satellite mission, and the accuracy of the discharge predictions at two virtual stations on the Torne River is explored.

# 2 Methods

The following sections will serve as an introduction to the field sites surveyed in Torne River, the conducted hydrometry surveys used for the hydraulic modelling, the setup of the hydraulic models, and an application of the models. Additionally, geodetic reference systems and flow in an open channel will be described shortly.

## 2.1 Field site

The Torne River is 520 km long, has catchment area of 39,775 km$^2$, and is one of Sweden's unregulated rivers [7]. The river originates from the lake called Torne träsk, which is located near the Norwegian border, and the river ultimately drains into the the Gulf of Bothnia [8]. Figure 1 shows an overview of the field site locations and the two areas of interest. In appendix 7.1, a map showing the location of the river and the two priority areas in Sweden, can be found. The city Övertorneå lies nearby priority area 1 (left), and the city Pello lies just upstream of priority area 2. The field site surveys were conducted from the 3rd to the 9th of September 2024.

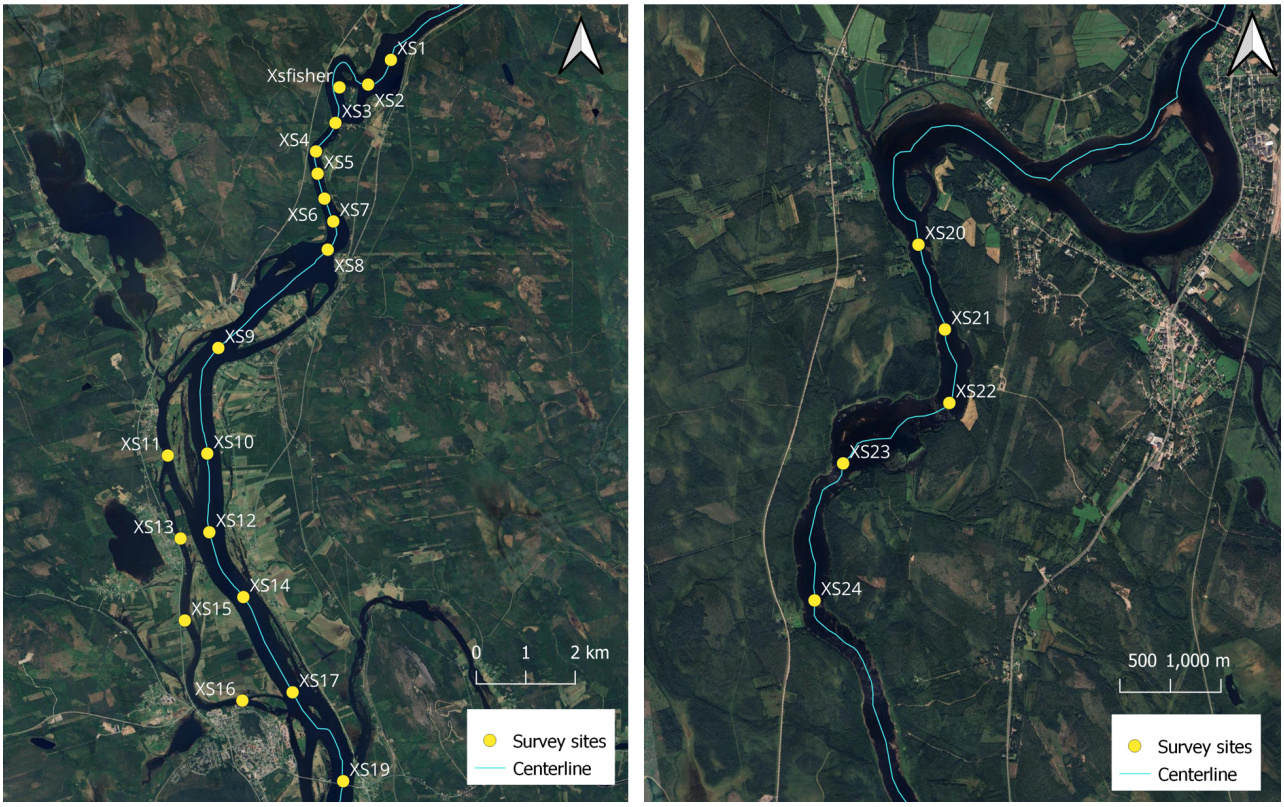


**Figure 1:** Overview of field sites (EPSG:3006). The left map is priority area 1 and the right map is priority area 2 (Original QGIS map is made by Zhen Zhou, Postdoc at DTU Space).

The locations of the surveyed cross sections are shown as the yellow dots, and in total 24 cross sections (XS) were surveyed. XS1 to XS19 are located in priority area 1, and XS20 to XS24 are located in priority area 2. The following table shows and an overview of the field sites. The focus of this project will mainly be on ground truth Water Surface Elevation (WSE) measurements using a Real-Time Kinematic (RTK) Global Navigation Satellite System (GNSS) receiver, Unmanned Aerial System (UAS) borne Water Penetrating Radar (WPR) bathymetry measurements and Surface Water and Ocean Topography (SWOT) satellite altimetry datasets. Therefore, the table only include if the RTK or WPR surveys has been conducted at each site. As table 1 shows ground truth measurements of the WSE has not been conducted at the tributary sites.

| **Site** | **Chainage [m]** | **Survey date** | **Surveys** | **Remarks** |
|---|---|---|---|---|
| XS1 | 90627.5 | 06-09-2024 | RTK, WPR | |
| XS2 | 91357.5 | 07-09-2024 | RTK, WPR | |
| XS3 | 93443 | 07-09-2024 | RTK, WPR | |
| XS4 | 94148.5 | 06-09-2024 | RTK, WPR | |
| XS5 | 94607.3 | 06-09-2024 | RTK, WPR | |
| XS6 | 95130.8 | 07-09-2024 | RTK, WPR | |
| XS7 | 95627.3 | 06-09-2024 | RTK, WPR | |
| XS8 | 96216.4 | 06-09-2024 | RTK, WPR | |
| XS9 | 99226.6 | 06-09-2024 | RTK, WPR | |
| XS10 | 101476.6 | 07-09-2024 | RTK, WPR | |
| XS11 | - | 04-09-2024 | WPR | Tributary |
| XS12 | 103067.9 | 07-09-2024 | RTK, WPR | |
| XS13 | - | 04-09-2024 | WPR | Tributary |
| XS14 | 104580.5 | 05-09-2024 | RTK, WPR | |
| XS15 | - | 05-09-2024 | WPR | Tributary |
| XS16 | - | 04-09-2024 | WPR | Tributary |
| XS17 | 106760.8 | 05-09-2024 | RTK, WPR | |
| XS19 | 108994 | 05-09-2024 | RTK, WPR | |
| XS20 | 54475.4 | 08-09-2024 | RTK, WPR | |
| XS21 | 55361.7 | 08-09-2024 | RTK, WPR | |
| XS22 | 56122.6 | 08-09-2024 | RTK, WPR | |
| XS23 | 57414.2 | 08-09-2024 | WPR | |
| XS24 | 58888 | 08-09-2024 | RTK, WPR | |

**Table 1:** Overview of the survey sites.

The area of interest (including both area 1 and 2) is surrounded by two in-situ gauging stations. The in-situ gauging stations, among other, measures discharge and water level [9]. One station is located in Pello, which is upstream of the area of interest, and the other station is located approximately 35 km dowstream of Övertorneå and is called Matkakoski. Table 2 shows the measured discharge on the survey dates at both in-situ stations.

| **Date** | **Discharge at Pello [m3/s]** | **Discharge at Matkakoski [m3/s]** |
|---|---:|---:|
| 04-09-2024 | 312.1 | 305.9 |
| 05-09-2024 | 306.9 | 295.5 |
| 06-09-2024 | 301.7 | 287.4 |
| 07-09-2024 | 295.9 | 280.4 |
| 08-09-2024 | 285.8 | 275.7 |

**Table 2:** Discharge on survey dates measured by in-situ stations [9].

As table 2 shows, the discharge at the downstream measuring station (Matkakoski) is generally lower than the discharge measured by the Pello station with a difference ranging from 6.2-15.5 $m^3/s$. The average discharge on the survey dates upstream of the area of interest (Pello), which is a discharge of 300.5 $m^3/s$, will be used for the hydraulic modelling.

## 2.2 Geodetic reference systems

The position of a point on the surface of Earth is defined in reference to a geodetic reference system, which is important to know, when working with geospatial data. A position of a point that contains information about latitude, longitude and elevation must be referenced to a three-dimensional reference system [10]. An example of a three-dimensional global reference system is the WGS84 that the GPS system and other Global Navigation Satellite Systems (GNSS) are referenced to [10]. In this project the swedish reference system, which is called SWEREF99 TM/RH2000, is used for positioning. SWEREF99 TM refers to the horizontal reference system (longitude and latitude positions), while RH2000 is the swedish national height system [10]. European Petroleum Survey Group (EPSG) codes are often used to represent different geodetic reference systems such as coordinate systems, ellipsoids and geoids [11]. The EPSG code for the SWEREF99 TM/ RH2000 system is EPSG:5845, the EPSG code for the horizontal SWEREF99 TM reference system is EPSG:3006, and the vertical EPSG code for the RH2000 height system is EPSG:5613 [12].

The elevation of a position is referenced to either a ellipsoid model or a geoid model. Both models are theoretical representations of the surface of Earth (so-called vertical datums). Ellipsoid models are mathematical models that assumes that the surface of Earth is smooth and

as the name states has the shape of an ellipsoid [13]. The WGS84 reference system is an example of an ellipsoid model [10]. The ellipsoid model does not take topography into account as it is completely smooth. Therefore, geoid models are often used to describe the surface of Earth more accurately. A geoid model uses the mean sea level to make a theoretical representation of the variations of Earth's surface elevation. The mean sea level is used because it responds to the gravitational pull of Earth. Geoid models are often made on a more local level compared to the ellipsoid models [14]. The height system used in Sweden is as mentioned called the RH2000. For the RH2000 system, the geoid model SWEN17_RH2000 can be used for converting an ellipsoidal height to a height above mean sea level (i.e. height above SWEN17_RH2000) [10]. When working with elevation data that is referenced to different reference systems, it is important to re-reference the elevation data to a common reference system to be able to compare the position data.

## 2.3 Ground truth WSE measurements

In-situ measurements of the WSE in the Torne River were carried out using an Emlid Reach RS3. The Emlid Reach RS3 is a Real-Time Kinematic (RTK) Global Navigation Satelitte System (GNSS) receiver. RTK GNSS is a positioning system that uses satellite signals to provide positioning information with a centimeter-level accuracy [15]. The accuracy of the RTK GNSS system is obtained as data from a network of fixed reference stations, is used. Based on known positions of the reference stations, satellite signals are monitored and corrected. An RTK GNSS reciever can use the corrections in real-time [15]. Thereby, accurate positioning data containing longitude, latitude and altitude can be measured using the RTK GNSS receiver, and the RTK GNSS system can thus be used to measure the WSE at each cross-section. Figure 2 shows how the WSE ground truth were measured, and as seen on the figure, the Emlid Reach RS3 receiver is placed on a rod, when surveying. The Emlid Flow app is used to collect the WSE at each cross-section, and three 15 second measurements are made at each survey site. In the Emlid flow app, the collecting mode was set to average over the 15 seconds. The RTK GNSS measurements are referenced to the SWEREF99TM/RH2000 reference system.

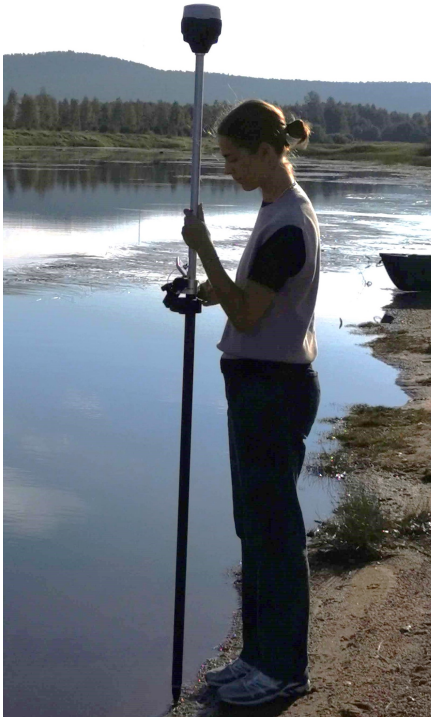

**Figure 2:** WSE measurements using an RTK GNSS reciever.

## 2.4 The Surface Water and Ocean Topography mission

The Surface Water and Ocean Topography (SWOT) mission aims to survey all of earths surface water. This includes measuring the water elevation of wetlands, major lakes, oceans and medium-to-large rivers (river reaches wider than 100 meters) [16]. SWOT has a 120 km wide swath and a 21-day repeat orbit, which results in that the SWOT mission on average provides data about land-based water bodies twice every 21 days [16]. The primary payload on the SWOT satellite is the Ka-band Radar Interferometer (KaRIn). The KaRIn is an altimeter, which measures the height of the water surface by emitting a cloud-penetrating radar signal. After the signal is emitted from the satellite, it hits the water surface and is reflected back to two antennas that are spaced 10 meters apart [17]. This allows for the satellite to collect data from two 50-kilometer wide swaths on both sides of the satellite [17]. In the gap between the two 50-kilometer wide swaths that KaRIn collects, a so-called Jason-Class Altimeter will collect water elevation. The Jason-Class Altimeter works by sending a signal that travels straight down and up, and then the travel time of the signal will be used to determine the water elevation [16]. Over land the system has a spatial resolution of 50 m and a heigth accuracy of 10 cm [18]. Additionally, there are larger uncertainties for pixels close to riverbanks, in areas with vegetation and near islands [19]. Figure 3 shows the SWOT satellite and the primary systems that allows the satellite to collect the water elevation data.

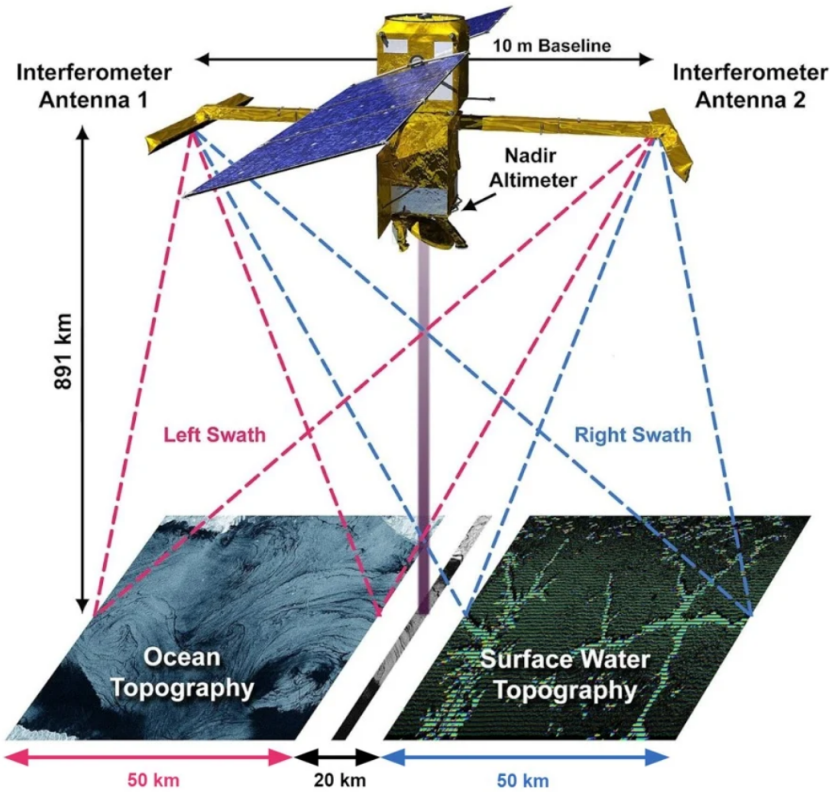


**Figure 3:** The SWOT satellite and the KaRIn dual-swath system [20].

### 2.4.1 Processing of SWOT data

The SWOT data is found on NASA Earth Data [21], where SWOT is selected under projects. Afterwards "SWOT Level 2 River Single-Pass Vector Data Product, Version C" is selected. The SWOT datasets that overlap the area of interest are selected. In the name of each dataset, a number which describes which area the dataset covers, is included. In this project, the Node datasets are used. During the field survey from the 3rd to the 9th of September 2024, two SWOT datasets covers the area of interest. These include the 456 dataset from 5th of September and the 484 dataset from the 484 dataset from the 6th of September. The SWOT data is referenced to the WGS84 reference system and the EGM2008 geoid. Thus, the data points from the selected datasets are re-referenced to the SWEREF99TM reference system and the RH2000 geoid.

## 2.5 Water penetrating radar

The following section will describe the Water Penetrating Radar (WPR) payload as well as the Unmanned Aerial System (UAS) platform and give an overview of how the processing of WPR data has been carried out. The WPR payload is a ground penetrating radar (GPR) payload, and the principle of GPR is that an electromagnetic wave is emitted by an antenna. The velocity of which the electromagnetic wave travels through a material, is mostly determined by the materials electric properties. Part of the electromagnetic wave is reflected back to a receive antenna, if the wave hits a layer with different electrical properties than the previous layer. The part of the wave that is not reflected back, keeps traveling downwards [22]. The GPR payload will further on be referred to as a WPR payload.

The WPR payload can be used to measure river bathymetry, which in other words is the bed elevation of the river. The drone-borne WPR provides information about the sub-merged river geometry (bathymetry), which is required for hydraulic modelling [23]. The study *Bandini et al.* (2023) showed that drone-borne WPR could measure bathymetry with an accuracy better than 0.1 m [3]. Furthermore, the study showed that the flight altitude should be approximately 0.5 m above the water surface. If the flight altitude is larger than 0.5 m above the water surface, the data will among other show a higher noise level [3].

### 2.5.1 UAS platform and payload

The water penetrating radar payload used in this project is based on the Zond Aero system from Radar Systems [24]. The payload as well as a GNSS receiver is carried by a DJI M300 RTK drone, which is an RTK-enabled Unmanned Aerial Vehicle (UAV) [25]. Thus, every WPR trace measurement has a location. Figure 4 shows the DJ M300 RTK drone carrying the WPR payload.

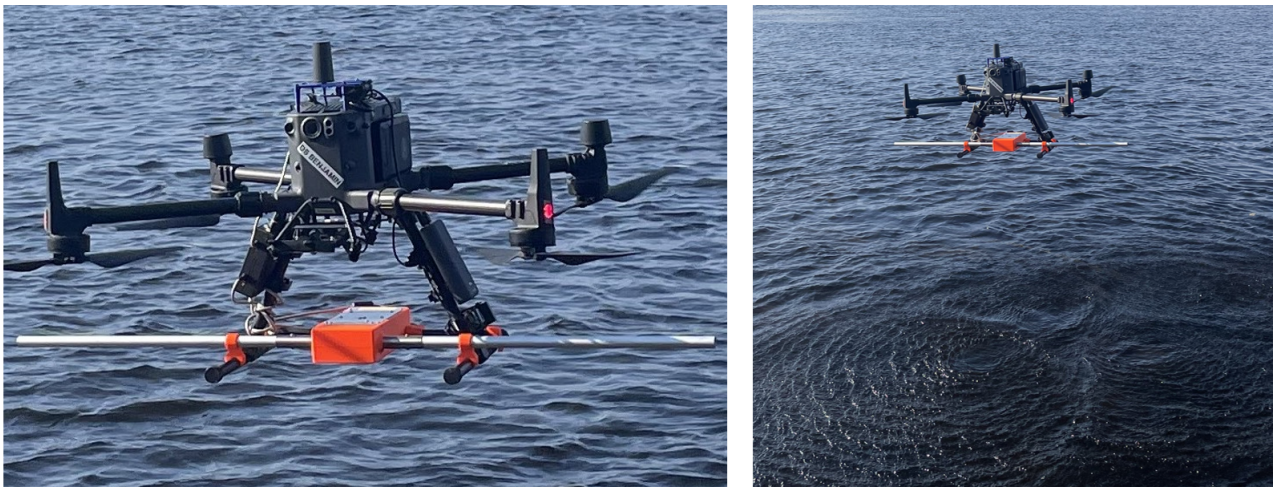

**Figure 4:** DJI M300 drone carrying WPR payload.

For the WPR surveying, a local base station, which provides RTK corrections to the drone, is set up. The corrections are provided to the drone via Starlink, which is a mobile broadband internet service provider [1]. A base station is a fixed GNSS reciever (here the Emlid RS3 is used) that has a known location [1, 15]. The base station can calculate real-time corrections of errors that can affect the positioning accuracy and transmit the corrections to the mobile receiver on the drone. It is assumed that the satellite signals travels with the speed of light, which might cause uncertainties due to atmospheric conditions. These uncertainties due to atmospheric conditions are examples of errors that can be corrected by the base station [26]. The elevation data is referenced to the WGS84 ellipsoid [1]. For rivers with a low electric conductivity (less than 250 $\mu\mathrm{S/cm}$) and with a depth that exceeds 0.8-1.1 m, the WPR payload can be used to measure river bathymetry [27]. Each cross-section has been overflown twice by the DJ M300 RTK drone.

### 2.5.2 Processing of raw WPR data

Figure 5 is the radargram for XS1 that shows the return signals from the riverbed. The x-axis shows the trace number and the y-axis shows the return time of the signals in nanoseconds [3].

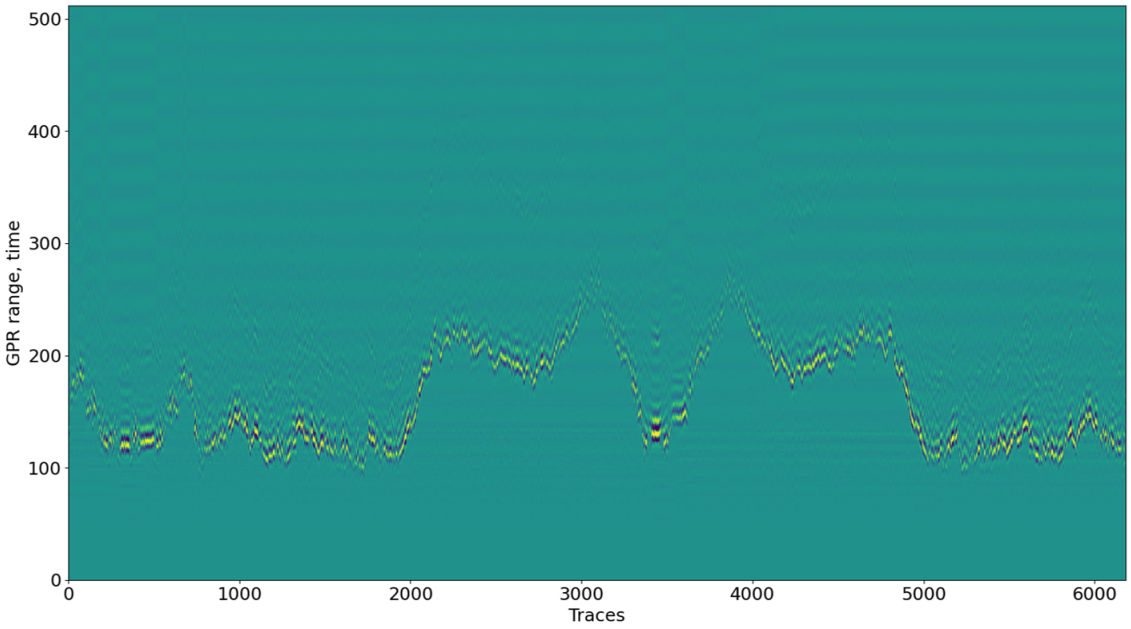


**Figure 5:** Radargram for XS1 that shows the return signals from the riverbed (WPR data from 06-09-2024). The y-axis shows the return time of the signals in nanoseconds.

The raw WPR data has been processed according to the method by *Bandini et al. (2023)* [3]. Firstly, the time-zero reference point is defined by determining the return signal from the water surface. Then a background removal filter is used to filter out noise in the signal. The WPR signal is then amplified, after which the bathymetry layer can be extracted. Next, the trace number values, GNSS coordinates, and return time, can be exported. Post-processed kinematic GNSS data is used to correct the coordinates in the bathymetry layer by using a relationship between trace number and timestamp (which is found in another file).

Hereafter, the depth can be determined from the return time of the riverbed using the GPR wave speed in water ($v_{water}$, see equation 2.1).

$$v_{water} \approx \frac{c}{\sqrt{\varepsilon_{water}}} \tag{2.1}$$

Here $c$ denotes the speed in vacuum and $\varepsilon_{water}$ is the relative permittivity of water (which is dependent on the water temperature [28]). Next, the water depth observations are converted from depth to bathymetry by subtracting the depth observations from the WSE measured by the RTK GNSS. The elevation of the river bottom is referenced to a datum, which in this project is the RH2000 geoid (EPSG:5613). The final step is to assign the bathymetric observations to points on the cross-section reference line. The cross-section reference line has been constructed by connecting a reference point on each bank of the river to each other. The processing of the raw WPR data for XS1 then results in the level 3 WPR data shown in figure 6. The processing of raw WPR data into level 3 WPR data has been conducted by Zhen Zhou (Postdoc, DTU Space) for all the cross-sections.

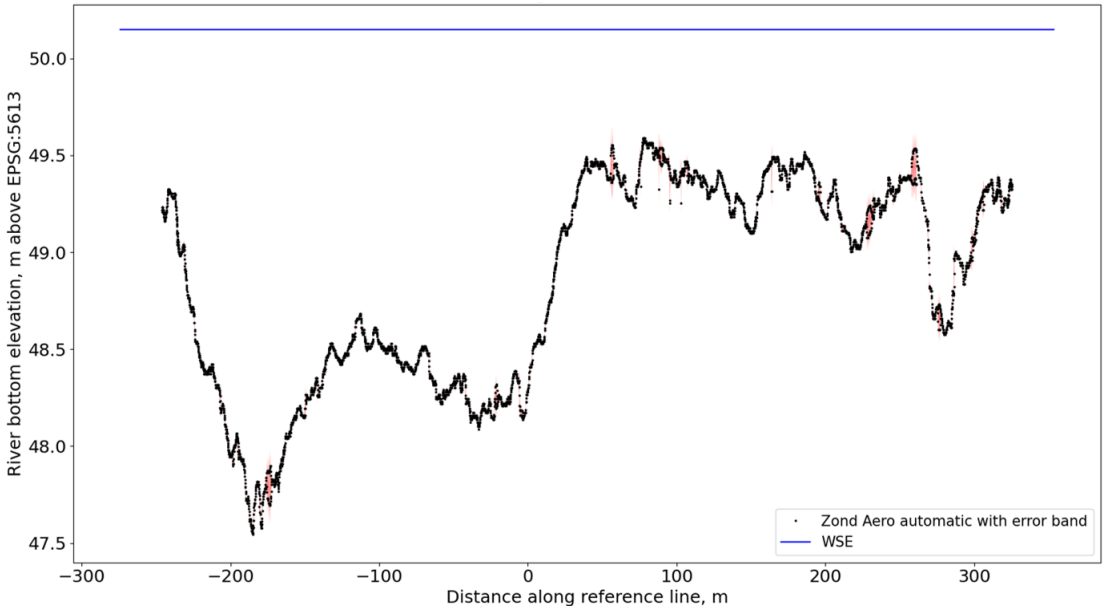


**Figure 6:** Level 3 processed WPR data.

### 2.5.3 Processing of level 3 WPR data

The processed level 3 WPR data contains data for the riverbed elevation for the submerged part of the river. However, as the WSE changes depending on the discharge in the river, the non-submerged parts of the cross-sections (i.e. the riverbanks) are derived from Digital Elevation Models (DEMs). Additionally, the WPR payload can only collect bathymetry data if the water depth exceeds 0.8-1.1 m, so bathymetry data is missing close to the riverbanks. Looking downstream the river, Sweden is on the right side of the river and Finland is on the left side of the river. For the Swedish (right) side of the river, the GLO-30 DEM, which is a Copernicus DEM with 30 meter resolution, is used to derive riverbank elevation data. The horizontal reference of the GLO-30 DEM is EPSG:4326 [29]. For the Finnish (left) side of the river, the open source Finnish elevation model with a resolution of 2 meters, is used to derive riverbank elevation data. The horizontal reference of the Finnish DEM is EPSG:3067 [30]. The horizontal coordinates for both DEM's are reprojected to the EPSG:3006, which is the horizontal reference system used in this project. Furthermore, both DEM's are re-referenced to the SWEN17_RH2000 geoid and thus the Swedish height system (RH2000). The re-referencing to the Swedish height system is done by adding the respective geoids that each DEM is referenced to and subtracting the SWEN17_RH2000 geoid from the DEM's. For the GLO-30 DEM, the EGM2008 geoid is subtracted and the SWEN17_RH2000 geoid is added. For the Finnish DEM, the N2000 geoid is added and the SWEN17_RH2000 geoid is subtracted.

After both DEM models have been re-referenced to the RH2000 geoid, it is possible to derive the elevation data of the non-submerged parts of the cross-sections. The cross-section

reference lines are extended to 1000 meter on each side of the centerline of the river. For the non-submerged parts of the Finnish (left) side, elevation from the re-referenced Finnish DEM are assigned to the points on the extended cross-section reference line. The same is done for the non-submerged parts of the Swedish (right) side of the river. However, for this side the elevation from the re-referenced GLO-30 DEM are assigned to the points on the extended cross-section reference line. This results in level 4 processed elevation data, and figure 7 shows an example of the processed data for XS1. A 1D smoothing spline fit it fitted to the WPR and DEM data, and the fit results in the level 4 processed elevation data (shown as a red line on the figure). The WPR and DEM data used for the fit is shown as the blue points behind the level 4 results.

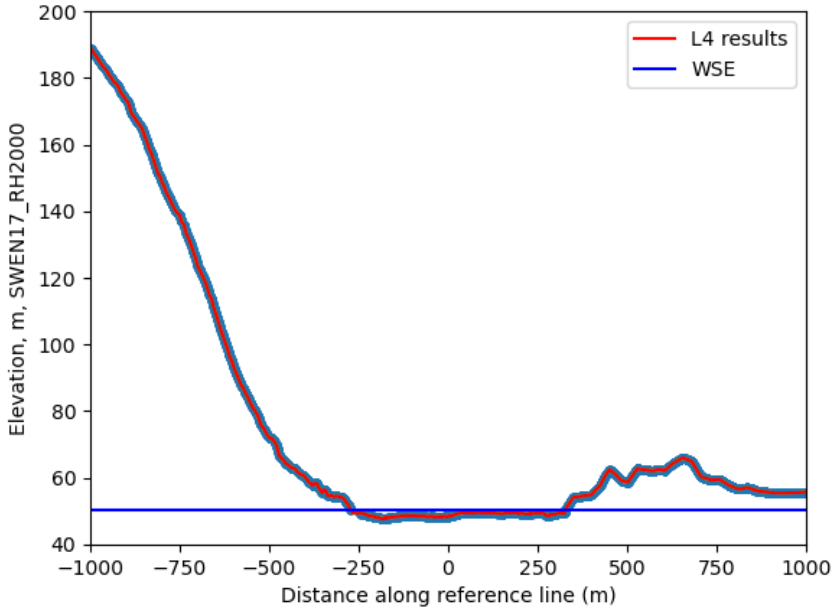


**Figure 7:** Level 4 processed WPR data for XS1.

For some cross-sections, the submerged bathymetry data from the WPR and non-submerged elevation data from the DEM's does not overlap. The reason for this can be a combination of missing bathymetry data close to the riverbanks, and that the WSE on the day of measuring elevation data for the DEM's has been higher than for the day of collecting WPR data [31]. The datagaps are handled by making a linear interpolation between DEM elevation data and the WPR bathymetry data. Figure 8 shows an example of this for XS5.

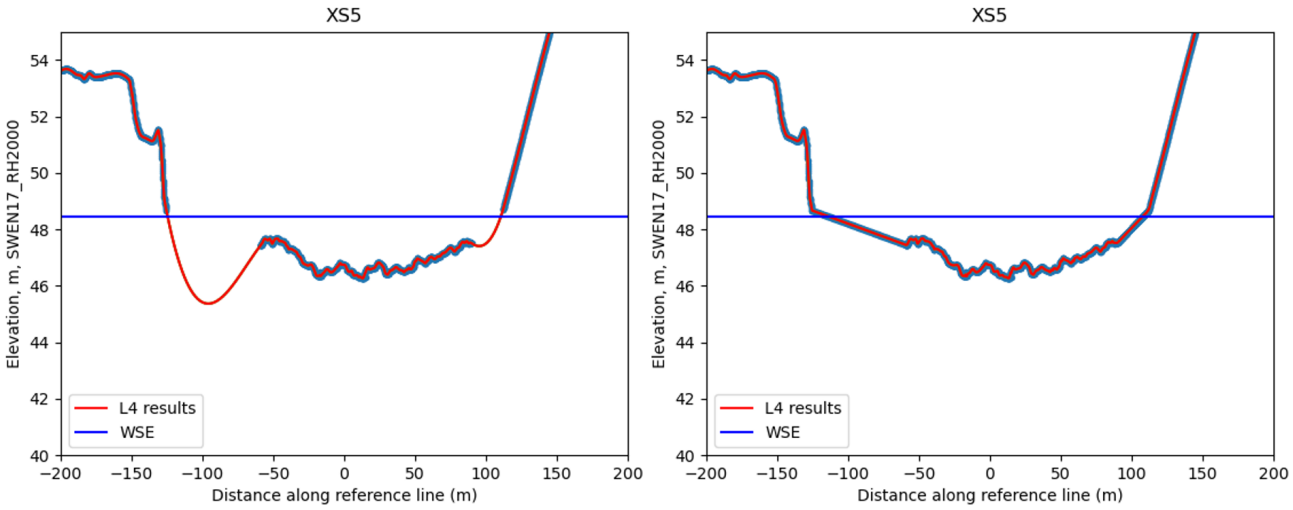


**Figure 8:** Example of handling of datagaps (XS5).

Furthermore, four cross-sections have two branches at the same chainage point, where WPR measurements have been made for each branch. Both hydraulic models that are computed in this project are one-dimensional, therefore the bathymetry data for the two branches has been combined. Point zero on the reference line is set to the centerline of the largest branch. Figure 9 shows an example of this, where the large branch is XS12 and the small branch is XS13. The small branch is located at a distance along the reference line of around 600 m.

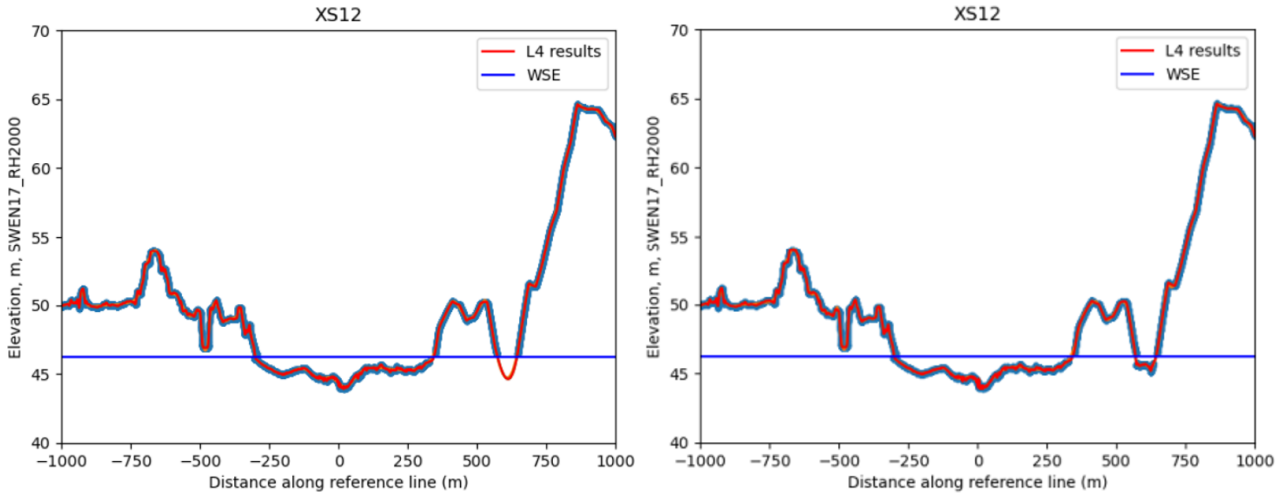


**Figure 9:** Example of handling of multiple branches, where XS12 is the large branch and XS13 is the small branch, which is located at a distance along the reference line of 600 m.

## 2.6 Flow in an open channel

In this project it is assumed that the flow in Torne river is steady and gradually varied. Steady flow means that flow depth at a specific chainage point does not change during a time interval. On the other hand, flow is unsteady, if flow depth changes with time. Additionally, flow is gradually varied, when the flow depth changes along the chainage over longer distances [32]. In some situations, uniform flow can occur in an open channel. For uniform flow to occur, the velocity, depth, discharge, and bed slope must be constant along the chainage and the cross-sections must be uniform for the section of the channel. In this situation, the slope of the water surface and the bed slope are parallel and thus the friction and gravity balance each other out ($S_f = S_0$) [33]. For uniform flow, the discharge is called the normal discharge and the corresponding depth is called the normal depth [33, 34].

The state of flow is affected by gravity, which is represented by the Froude number:

$$\mathrm{Fr} = \frac{v}{\sqrt{g \cdot w}} \tag{2.2}$$

$Fr$ is the Froude number, which is dimensionless, $v$ is the mean velocity of the flow [m/s], $g$ is the acceleration of gravity [m/s$^2$], and $w$ is the flow depth [32]. The term $\sqrt{g \cdot w}$ represents the speed of gravity waves in shallow water [34]. If the mean flow velocity is equal to the speed of the gravity waves for a given section in the river, the Froude number is equal to 1 and the state of the flow is *critical* [32]. If the mean flow velocity is less than the speed of the gravity waves for a given section in the river, the Froude number is less than 1 and the state of the flow is *sub-critical*. Sub-critical flow is associated with larger depth and lower velocities [34]. Lastly, if the mean flow velocity is larger than the speed of the gravity waves for a given section in the river, the Froude number is larger than 1 and the state of the flow is *super-critical*. Super-critical flow is associated with smaller depths and higher velocities [34]. Sub-critical flow will occur on channels with a mild bed slope, while super-critical flow will occur on channels with a steep bed slope [34].

The state of the flow is important to know, when computing the WSE for a river reach. For sub-critical flow conditions, changes downstream in the river can affect the flow upstream as the flow velocity is less than the speed of the gravity waves. Thus, for sections with sub-critical flow, the WSE must be computed starting downstream in the section and moving upstream. Opposite to this, the downstream changes in a river does not affect the upstream flow under super-critical flow conditions as the flow velocity is higher than the speed of the gravity waves. Thus, for sections with super-critical flow, the WSE must be computed starting upstream in the section and moving downstream [31].

In open channels, different local phenomena might happen, which are changes that take place over short distances [35]. A hydraulic drop is an example of a local phenomena. Here

the flow depth changes from high to low often due to changes in the bed slope or cross section, which results in a steeper water surface slope [35]. A special case of the hydraulic drop is the so-called *free overfall*. Here the bottom of the channel is discontinued, resulting in a drop of the WSE. If a pool is created by for example a dam or due to the shape of the river bottom, an overfall can occur when the water flows over the dam or an elevated part of the river bottom [36]. Figure 10 shows an example of this, where the upstream channel has a subcritical slope:

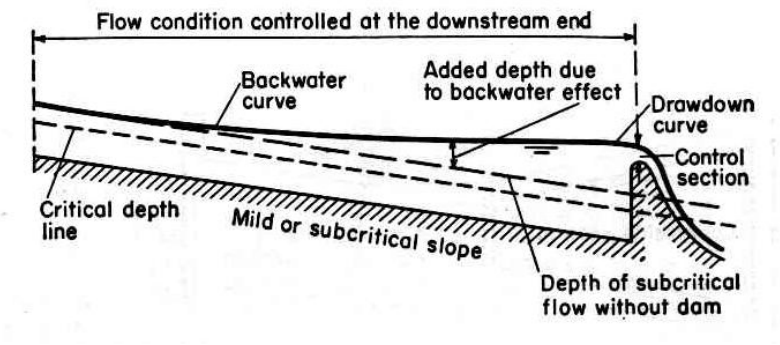


**Figure 10:** Flow conditions in a long channel with a mild bed slope [36].

As shown on the figure, a control section is marked at the edge of the overfall (edge of the dam). A control section is a specific location in a channel, where a definitive relationship between the WSE and discharge is found [36]. The location and shape of the cross section of the control section is important to know, when simulating the WSE along a river reach, because the WSE is determined by the control section [31].

## 2.7 Hydraulic model of the WSE

In this project, two hydraulic models have been set up for each priority area; one using a Steady-State (SS) solver and one using the MIKE+ software. Both hydraulic models solve the governing equations numerically.

### 2.7.1 Steady-state solver

In the study *Kittel et al.* (2021), a Steady-State solver based on the Saint-Vernant equations that simulates the the WSE along a river reach at a given discharge, was developed [5]. The one-dimensional Saint-Vernant equations, which includes the continuity and the momentum equation, are used to set up the SS-solver. The SS-solver is based on one-dimensional Saint-Vernant equations for steady, gradually varied flow in an open channel and with the assumption of no lateral inflow. With these assumptions, the derivative of the water depth as a function

of chainage can be described as:

$$\frac{dh}{dx} = \frac{\left(\frac{Q^2}{g \cdot A^3}\frac{\partial A}{\partial x} + S_0 - \frac{Q^2}{K^2}\right)}{\left(1 - \frac{Q^2}{g \cdot A^3}\frac{\partial A}{\partial h}\right)} \tag{2.3}$$

Where $h$ is water depth in the channel [m], $x$ is the chainage [m], $Q$ is the discharge [$m^3/s$], $g$ is the gravitational acceleration [$m/s^2$] (here set to 9.82 $m/s^2$), $A$ is the cross-sectional area [$m^2$], $S_0$ is the bed slope of the river [m/m], and $K$ is the conveyance [$m^3/s$]. To calculate the WSE along the chainage a downstream WSE boundary condition is needed to initialize the SS-solver [5]. The computation of the downstream boundary conditions for the two areas are described in section 2.7.3. The WSE can then be calculated starting at the downstream boundary condition and moving upstream along the chainage in stepwise spatial increments ($\Delta$x) by solving equation 2.4 [5]:

$$h_{i-1} = h_i - RHS\left(x_i, h_i\right) \cdot \Delta\mathrm{x} \tag{2.4}$$

*RHS(x,h)* denotes the right hand side of equation 2.3. When using the SS-solver, the spatial increments are set to 1 m, which are rather small increments. However, equation 2.4 requires small $\Delta$x steps to be stable [5], and the computation time is still low. Furthermore, the level 4 processed cross-sections are stored in and retrieved from the cross section module in MIKE+, where they are defined at their respective chainage points. Cross section information is interpolated in between cross sections with information about cross sectional geometry (WPR and DEM data), when using the cross section module in MIKE+ [31].

### 2.7.2 Hydrodynamic model using MIKE+

In MIKE+, a hydrodynamic model of the WSE along the river, can be set up using the 1D computational engine. The 1D computational engine can be used for modelling unsteady flows in river networks based on a numerical solution to the one-dimensional Saint-Vernant equations [37]. The fully dynamic higher order wave approximation is used for the hydrodynamic modelling of the WSE. The 1D engine can both compute sections with sub-critical flow and sections with super-critical flow. The accuracy of the Saint-Vernant equations in the fully dynamic wave approximation is high for sub-critical flow. However, simplifications are used to increase stability for the computation of the sections with super-critical flow conditions. Thus, the 1D solution is less accurate at high Froude numbers than at lower Froude numbers [37].

When setting up the hydrodynamic model in MIKE+, the L4 processed cross-section data is as well as a shape-file containing the river centerline is imported into MIKE+. The cross-sections are defined for their respective chainage points along the river centerline. For priority area 1, the maximum spatial increments are set to 200 m

Two boundary conditions are used: a downstream river water level of 45.94 m above EPSG:5613 and an open inflow to river of 300.5 $m^3/s$. The initial condition is set to 2 m, and the simulation period is set to 10 days. For this simulation period, the model is not sensitive to the initial condition. Adaptive time steps are used with a minimum of 5 seconds, maximum of 60 seconds and a maximum increase factor of 1.1. Together with the simulation period, the adaptive time steps results in a stable model without random fluctuations and the model reaches steady-state. Furthermore, the Manning $n$ formulation is used to define the bed roughness, and the default roughness is set to 1 $s/m^{1/3}$. However, for every section of the river a roughness factor is multiplied with the default bed roughness, resulting in Manning numbers ranging from 0.023-0.10 $s/m^{1/3}$. These Manning numbers have been calibrated using the SS-solver.

For priority area 2, the maximum spatial increments are set to 60 m. Two boundary conditions are used: a downstream river water level of 72.07 m above EPSG:5613 and an open inflow to river of 300.5 $m^3/s$. The initial condition is set to 0.4 m, and the simulation period is set to 10 days. Adaptive time steps are used with a minimum of 5 seconds, maximum of 10 seconds and a maximum increase factor of 1.1. Together with the simulation period, the adaptive time steps results in a stable model without random fluctuations and the model reaches steady-state. Here, the Manning $n$ formulation is also used to define the bed roughness, and the default roughness is set to 1 $s/m^{1/3}$. However, for every section of the river a roughness factor is multiplied with the default bed roughness, resulting in Manning numbers ranging from 0.030-0.16 $s/m^{1/3}$.

### 2.7.3 Boundary conditions

As mentioned the downstream WSE boundary conditions must be calculated, in order to initialize the SS-solver. Additionally, the boundary conditions are used when computing the WSE using the MIKE+ software. It is assumed that there are uniform flow conditions downstream of the two priority areas. As mentioned, it can at uniform flow be assumed that the bed slope is equal to the friction slope. With this assumption, Mannings equation for the friction slope can be rewritten as follows:

$$S_f = \frac{n^2 \cdot Q^2}{A^2 \cdot R_H^{\frac{4}{3}}} \Rightarrow S_0 = \frac{n^2 \cdot Q_n^2}{A^2 \cdot R_H^{\frac{4}{3}}} \tag{2.5}$$

Here $S_f$ is the friction slope [m/m], $n$ is the Manning parameter [$\mathrm{s/m^{1/3}}$], $Q$ is the discharge [$m^3/s$], $A$ is the cross-sectional area [$m^2$], $R_H$ is the hydraulic radius [m], $S_0$ is the bed slope [m/m], and $Q_n$ is the normal discharge [$m^3/s$].

In the MIKE+ software an expression that describes the relationship between the water level and the flow area as well as an expression that describes the relation between the water

level and the hydraulic radius can be retrieved. It is assumed that the cross sectional geometry downstream of the last cross section with WPR/DEM data, is equal to the geometry of this last cross section. Therefore, the relationship between water level and the flow area and the relationship between the water level and the hydraulic radius for the most downstream cross-section, can be set into equation 2.5. The relationships for XS19, which is the last cross-section in priority area 1, are as follows:

$$A = 44.19 \cdot WSE^2 - 3203 \cdot WSE + 55522 \tag{2.6}$$

$$R_H = 0.6917 \cdot WSE - 29.89 \tag{2.7}$$

The relationships for XS24, which is the last cross-section in priority area 2, are as follows:

$$A = 32.18 \cdot WSE^2 - 4229 \cdot WSE + 137672 \tag{2.8}$$

$$R_H = 0.671 \cdot WSE - 46.54 \tag{2.9}$$

In appendix 7.2, the relationships for XS19 and XS24 are shown as graphs. Furthermore, the downstream bed slope ($S_0$) is estimated. For priority area 1 this is done by extracting the lowest riverbed elevation point for cross-section 9, 10, 12, 14, 17, and 19 (i.e. the last 6 cross-sections in priority area 1). The lowest riverbed elevation points extracted from cross-section 9 and 19, are determined to be outliers. Thus, a linear regression using the remaining 4 points is made, and from this the downstream bedslope is determined to be 0.023 m/km (view appendix 7.2).

Less field sites has been surveyed at priority area 2. A linear regression is thus made between the lowest riverbed elevation point for the two most downstream cross sections in area 2 (XS23 and XS24). From these riverbed elevation point, a bed slope is determined to be 1.11 m/km. From the SWOT 456 dataset it seems that the downstream bed slope is steeper compared to the calculated bed slope. The downstream bed slope (and Manning $n$) used to calculate the downstream WSE boundary condition has been calibrated against the WSE measured at XS24. This yielded a downstream bed slope of 11.1 m/km.

The ground truth WSE measurements using the RTK GNSS receiver and the WSE measured by the WPR differs by 17.5 cm for XS24, which is the most downstream cross-section in priority area 2. Thus, the downstream WSE boundary condition for the hydraulic model at area 2, is calculated based on XS24. The riverbed elevation of the cross-sections is determined based on a depth measured by the WPR (i.e the WSE is the point zero and the riverbed elevation is then determined based on the depth of the riverbed). The WPR measurement of the WSE for XS24 is 17.5 cm above the ground truth measurement of the WSE, which might pose a problem when modeling the WSE and calculating the boundary condition. As the ground truth RTK measurement are consistent with the 456 SWOT data from September 5th 2024, it is assumed

that the ground truth RTK measurement of the WSE is more accurate. Therefore, 17.5 cm has been subtracted from the riverbed elevation in each bathymetry point (for the submerged part of the cross section). This results in a more stable boundary condition for priority area 2 (and when calibrating the model, the Manning $n$ is 0.03 instead of 0.01).

### 2.7.4 Model calibration

The bed roughness at different sections of the river is calibrated by trial and error using the steady-state solver. The hydraulic model computed by the SS-solver is calibrated against the SWOT 456 WSE observations as this dataset shows the best correlation with the RTK ground truth measurements. Additionally, the SWOT 456 dataset covers both priority areas, which the SWOT 484 dataset does not. Each priority area is divided into 5 sections, where different Manning numbers are assigned to after calibration.

Furthermore, for priority area 1 a virtual cross-section is insertet at chainage x=95900 m. The upstream cross-section at chainage x=95627.3 m (XS7) is copied and inserted at x=95900 m, and thus it is assumed that the virtual cross-section has the same cross-sectional geometry as XS7. The insertion of a virtual cross-section is made to better simulate an overfall that seems to happen approximately after x=95900 m. Inserting the virtual cross-section is a way of calibrating the model, so that it is able to simulate the overfall and get closer to the SWOT 456 observations of the WSE at XS8, which is downstream of the overfall.

## 2.8 Model application: Virtual station using data from Sentinel-3

The hydraulic models can be used to construct rating curves for different chainage point along the river. A rating curve shows the relationship between water level and discharge in the river [34]. This relationship can be simulated using the calibrated hydraulic models by simulating the water level at different given discharges at one location on the river. A rating curve can then be fitted to the simulated relationship between water level and discharge points. From a rating curve a given water level can be used to estimate the discharge [34]. Thus, WSE measurements observed by satellites can be converted to discharge each time the satellite passes the river at a so-called virtual station [23].

A virtual station is the intersection of a satellite ground track with the river [38]. In this project a virtual station is developed using data from the Sentinel-3 satellite mission. The observations made by the Sentinel-3 mission among other include river water surface height, which are the observations that are used in this project. There are two satellites in orbit in the Sentinel-3 mission (the Sentinel-3A and the Sentinel-3B), which are identical and have identical orbits, which are just shifted in relation to each other. The spatial resolution of the mission is 300 m. Furthermore, the satellites have a ground track deviation of +/- 1 km, which

means that the ground track is not located at the excact same position at each passage [39]. When making a virtual station using the Sentinel-3 data, the virtual station is thus located in a defined area on the river in the range, where the ground track of the Sentinel-3 satellite is located. From the Sentinel-3 WSE observations and the rating curves constructed at the specific chainage points using the hydraulic models, a river discharge time series is made.

### 2.8.1 Processing of Sentinel-3 data

A Sentinel-3 dataset that among other contains timestamp, longitude, latitude and WSE, has been provided by the UAWOS team. The Sentinel-3 data is referenced to the WGS84 reference system and the EGM2008 geoid. Thus, the data points are re-referenced to the SWEREF99 TM reference system and the RH2000 geoid. Then, the sentinel-3 data is sorted and data points further away than 200 meters from the centerline are excluded. Additionally, values for the WSE that are above 80 m above EPSG:5613 are also excluded as these are assumed to be ground elevations or errors. Lastly, as the river is likely frozen in winter, the sentinel-3 data measured between December 1st and April 31st, are also sorted out. Each data point is connected to the closest chainage value on the centerline. Rating curves are made based on the SS-solver for each chainage point, where sentinel-3 data is measured. The rating curves are made for a discharge range of 84-2500 $m^3/s$ for area 1, and a discharge range of 150-2500 $m^3/s$ for area 2. A polynomial function is fitted to the rating curve, and from the fitted rating curve, discharge data to a corresponding WSE value can be retrieved. The Sentinel-3 WSE data is used to retrieve corresponding discharge data from the rating curves. When discharges are retrieved based on the rating curves, a time series is made, where discharge is on the y-axis and time is on the x-axis. The predicted discharge is compared to the discharge measured on the same dates at the Pello measuring station.

# 3 Results

In the following sections, the results obtained are showed and described. This include the results of the level 3 WPR data processing, the two hydraulic models for each priority area, evaluation of the hydraulic models, and the model application results.

## 3.1 Riverbed elevation data for cross sections

All 23 cross sections (no WPR data for XS18) have been processed in accordance to section 2.5.2 and 2.5.3. The results for each cross section can be found in appendix 7.4. However, the cross sections that needed additional processing due to for example datagaps or multiple branches are shown here. Besides XS5, four other cross sections had datagaps, where linear

interpolations have been made between WPR data and DEM data. These cross sections include XS7, XS8, XS9, and XS24, which are shown on figure 11.

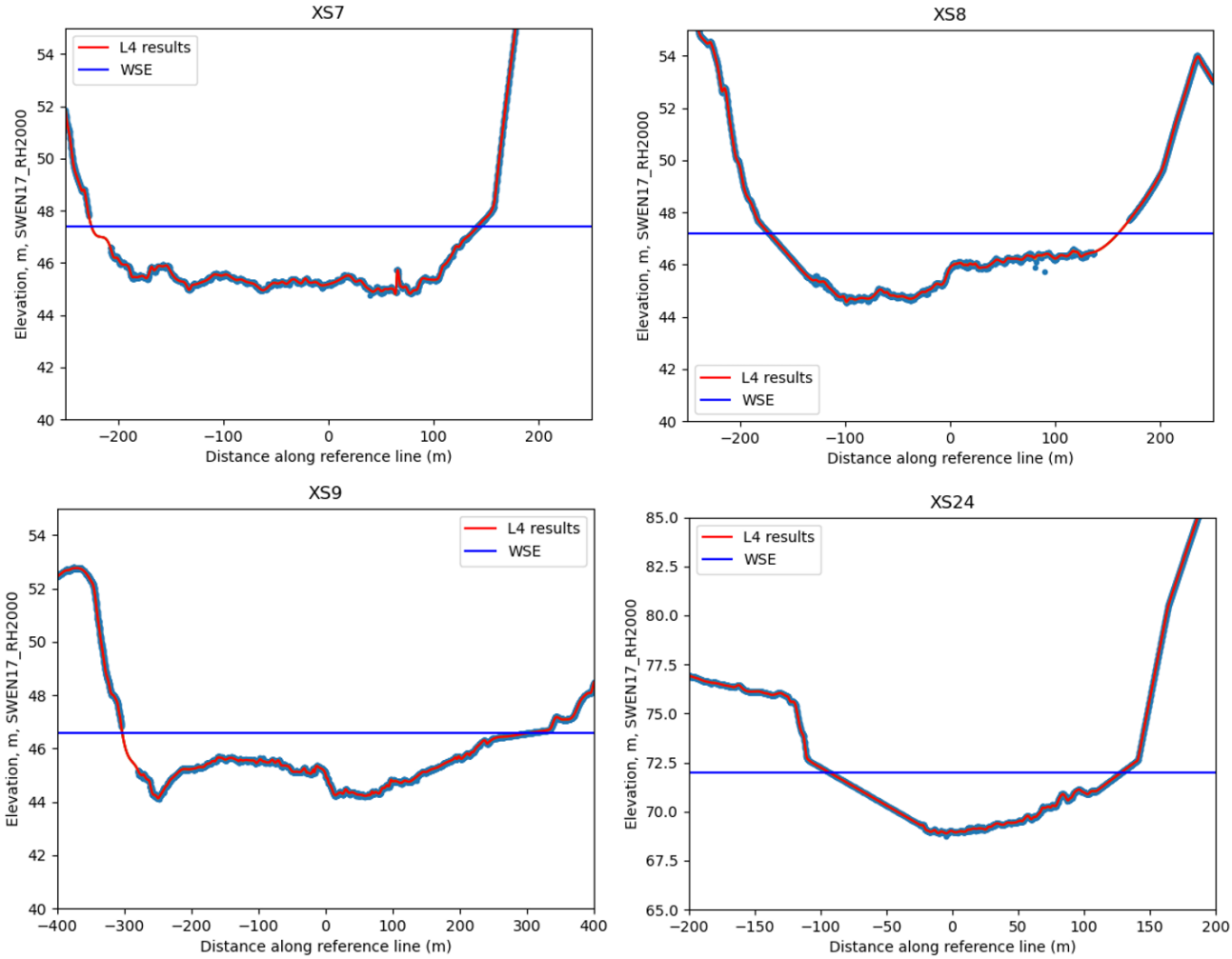


**Figure 11:** Cross sections where datagaps has been handled using linear interpolations.

As mentioned, four cross section have two branches at the same chainage point. Besides XS12, this incudes XS10, XS17, and XS19. Figure 12 shows the results of the cross section processing of XS10 and XS17, which are both the largest branches at their respective chainage points. The small branch at the same chainage point as XS10 is XS11, and the small branch at the same chainage point as XS17 is XS16.

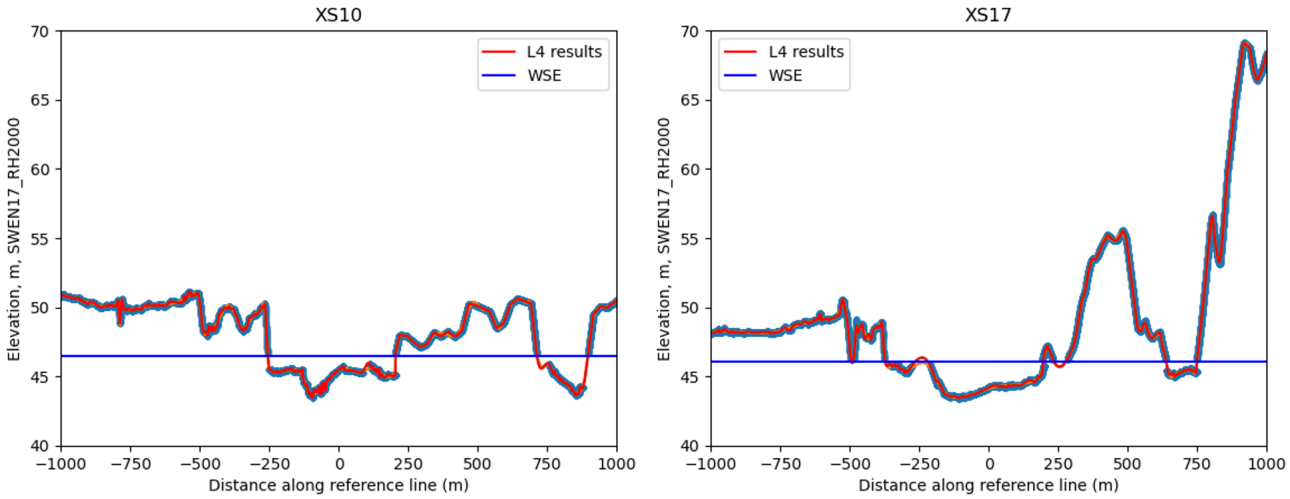


**Figure 12:** Cross sections (XS10 and XS17) with two branches at same chainage point.

The reference lines are made in reference to the centerline of the largest branch at the chainage point. However, this results in that the reference line does not completely overlap the cross section at the small branch of the chainage point. Figure 13 shows XS17, XS16 and the reference line made for XS17. As the figure shows, the reference line does not overlap XS16 (this is the cross section, where the distance between the small branch cross section and the reference line is furthest apart). Even though, the reference line and XS16 does not overlap, the WPR data from XS16 is inserted at the location, where the reference line crosses the tributary. This is the best available estimate of how the bathymetry of the tributary at the reference line is.

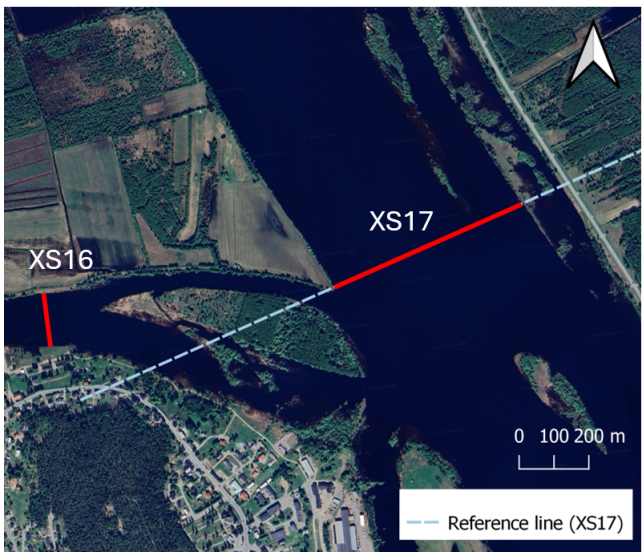


**Figure 13:** Map showing XS16 and XS17 (EPSG:3006) and the reference line used to construct the cross section elevation data of XS17.

As mentioned, no WPR data has been measured for XS18, which is a tributary located at the same chainage point as XS19. Thus, the submerged part of the tributary is extrapolated using a 1-D smoothing spline fit. The resulting elevation data for XS19 is shown in figure 14.

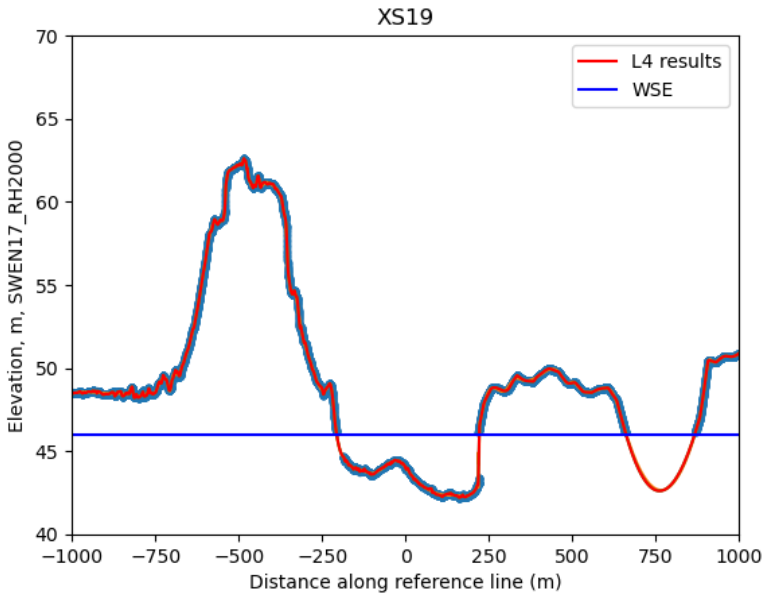


**Figure 14:** Elevation data for XS19, where no WPR data has been measured for the tributary (XS18).

## 3.2 Hydraulic models

### 3.2.1 Results of bed roughness calibration

The hydraulic model computed with the SS-solver has been used to calibrate the Manning numbers along the river reach, resulting in Manning numbers of 0.023-0.10 $s/m^{1/3}$ for area 1, and 0.03-0.16 $s/m^{1/3}$ for area 2. Figure 15 shows the different sections in each priority area and their respective Manning numbers used in the computation of the hydraulic models. The Manning numbers have been calibrated against SWOT 456 observations.

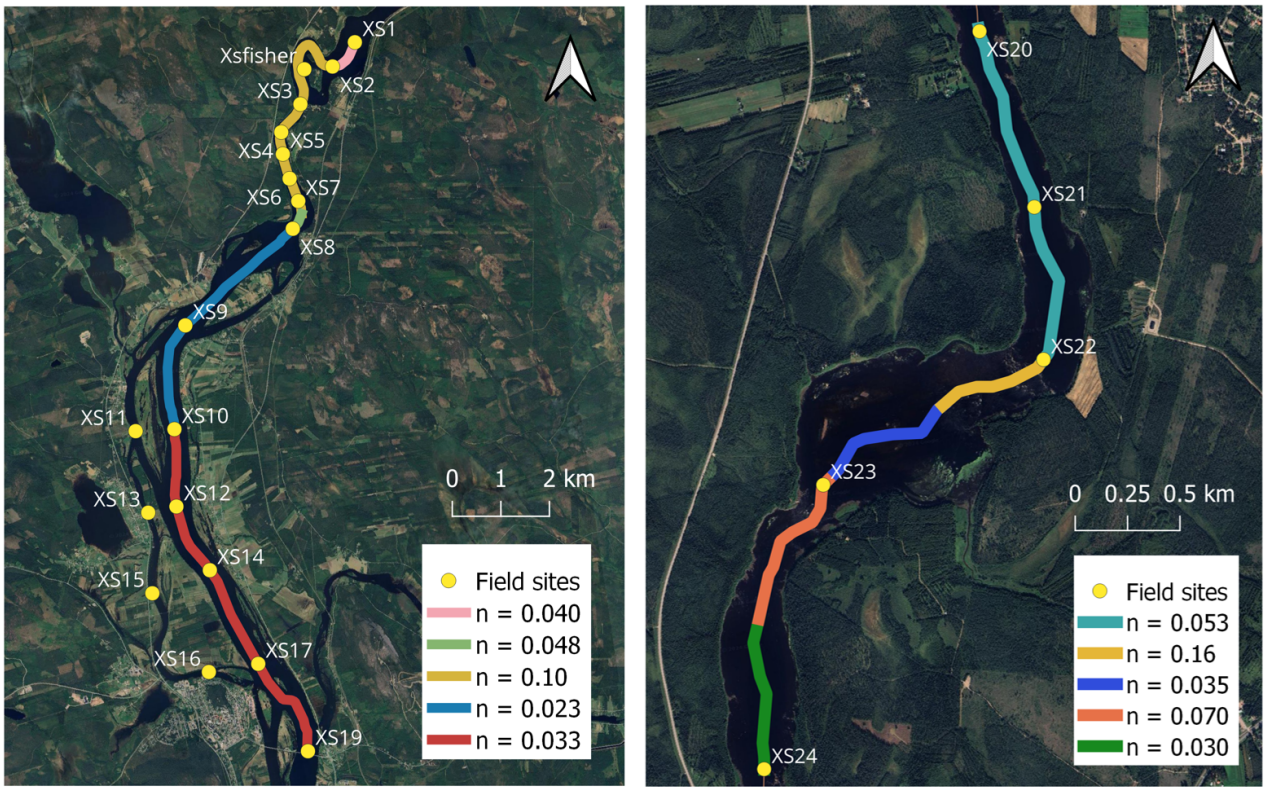


**Figure 15:** Map showing the results of Manning *n* calibration (EPSG:3006).

### 3.2.2 Priority area 1

Two hydraulic models of the WSE have been set up for priority area 1 - one using the steady-state solver and one using the MIKE+ software. The downstream WSE boundary condition has been determined to to 45.94 m above EPSG:5613 for a discharge of 300.5 $\mathrm{m}^3/\mathrm{s}$. Figure 16 shows the two models along with the ground-truth RTK measurements of the WSE, the SWOT 456 observations, and the SWOT 484 observations. As mentioned, the SS-solver has been calibrated against the SWOT 456 observations of the WSE by adjusting the Manning numbers for different sections of the river. The same Manning numbers have been used in the MIKE+ model. As shown on figure 16 the hydraulic model results computed using the steady-state solver are nearly identical to those obtained with the MIKE+ software. Additionally, figure 16 shows that the model results are consistent with the RTK WSE measurements and the both SWOT datasets.

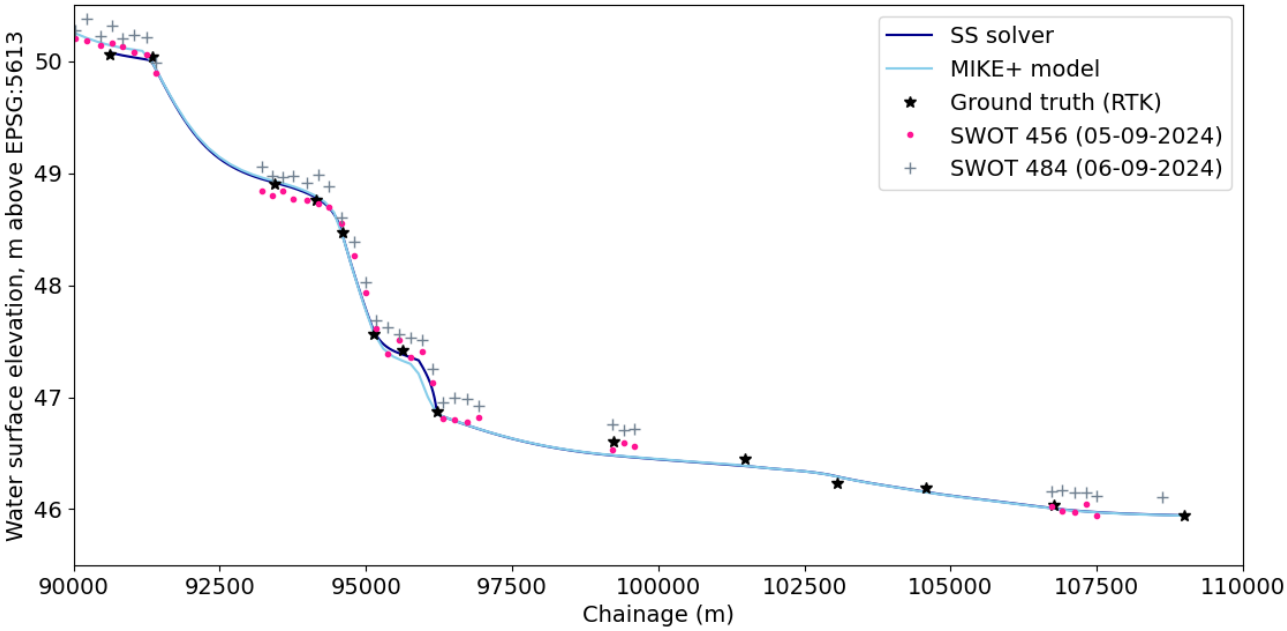


**Figure 16:** Hydraulic model of WSE for area 1 using SS-solver and MIKE+ compared with ground truth WSE measurements and SWOT-data from survey dates.

The Froude numbers along the chainage are computed for each of the hydraulic models, and the results are shown in figure 17. As the figure shows, there is a shift in the Froude numbers computed with the SS-solver compared to the Froude numbers computed in MIKE+. However, the same pattern is seen for the Froude numbers for the two models. Furthermore, figure 17 shows that all Froude numbers are below one.

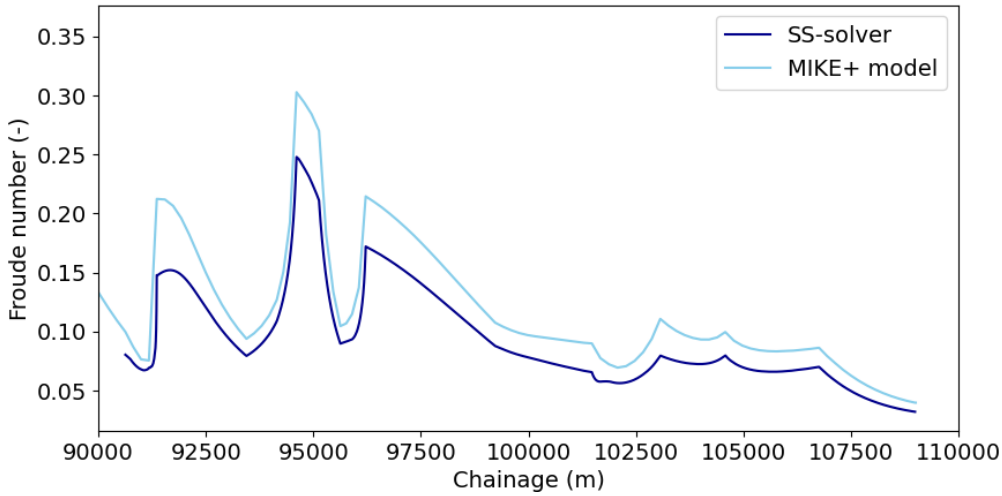


**Figure 17:** Froude numbers for area 1 along the chainage for the two hydraulic models.

### 3.2.3 Priority area 2

Two hydraulic models of the WSE have also been set up for priority area 2. The downstream WSE boundary condition has been determined to to 72.07 m above EPSG:5613 for a discharge of 300.5 $\mathrm{m}^3/\mathrm{s}$. Figure 18 shows the two models along with the ground-truth RTK measurements of the WSE and the SWOT 456 observations. The 484 SWOT dataset does not cover priority area 2, and is therefore not included. Two WPR WSE measurements has also been included in the figure. The WPR WSE measurement at chainage 57400 is included as the ground truth RTK WSE was not measured at this cross section. However, WPR data was measured at this chainage point. The WPR WSE at chainage 58900 (XS24) is included to show the difference between the WSE measured by the RTK GNSS receiver and the WSE measured by the WPR at this site. For priority area 2 the hydraulic model results computed using the steady-state solver are also nearly identical to those obtained with the MIKE+ software. However, the two models differs from each other at chainage 56100-56600. Additionally, figure 16 shows that the model results are generally consistent with the RTK WSE measurements and the 456 SWOT dataset.

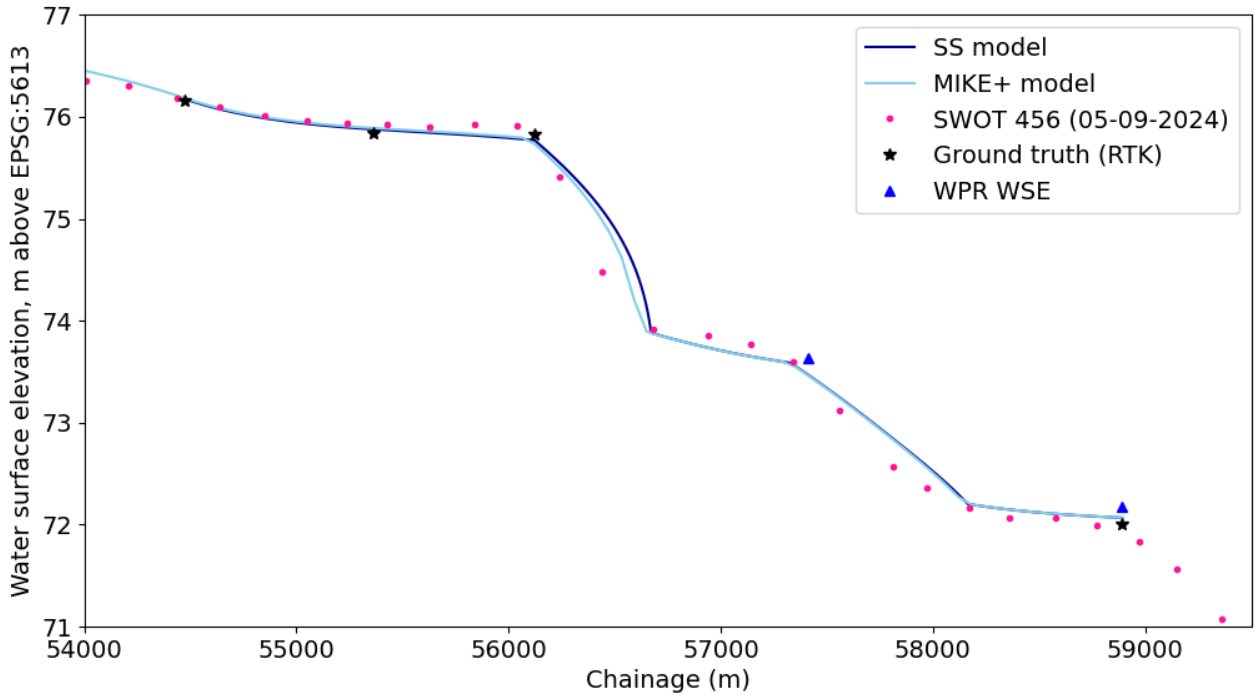


**Figure 18:** Hydraulic model of WSE for area 2 using SS-solver and MIKE+ compared with ground truth WSE measurements and SWOT-data from survey dates as well as two WPR WSE measurements.

Additionally, the Froude numbers along the chainage have been computed for each of the hydraulic models, and the results are shown in figure 19. As for priority area 1, there is a shift in the Froude numbers computed with the SS-solver compared to Froude numbers computed

in MIKE+. Additionally, the same pattern is seen for the Froude numbers for the two models. Furthermore, figure 19 shows that all Froude numbers are below one.

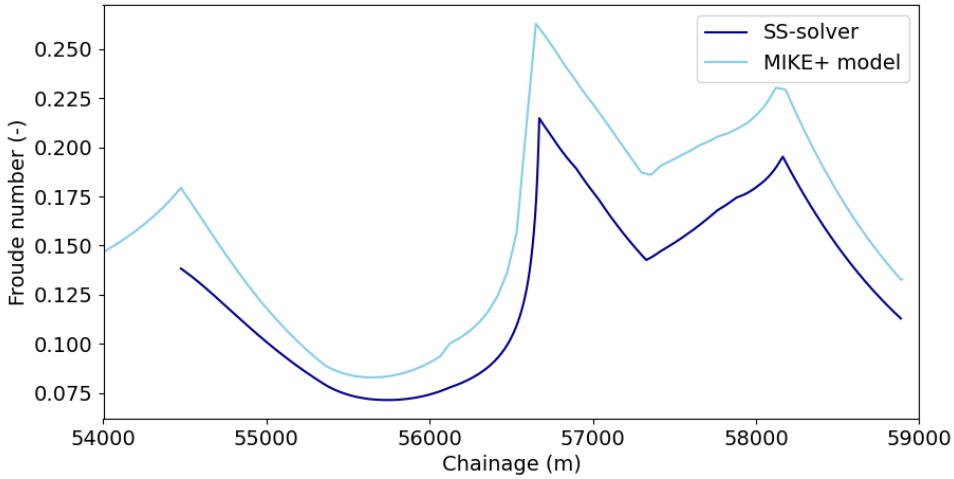


**Figure 19:** Froude numbers for area 2 along the chainage for the two hydraulic models.

### 3.2.4 Error metrics

Three error metrics have been calculated to compare the simulated WSE from the hydraulic models with the ground-truth RTK measurements of the WSE as well as the WSE from the 456 and 484 SWOT datasets. The three error metrics are Root Mean Square Error (RMSE), Mean Bias Error (MBE), and Mean Absolute Error (MAE) [40]. The error metrics have been calculated using the following three formulas. In the formulas $\hat{y}$ denotes the predicted model value and $y$ denotes the measured value (either ground truth RTK or SWOT value).

$$RMSE = \sqrt{\frac{1}{n}\sum_{i=1}^{n}(\hat{y}_i - y_i)^2} \tag{3.1}$$

$$MBE = \frac{1}{n}\sum_{i=1}^{n}(\hat{y}_i - y_i) \tag{3.2}$$

$$MAE = \frac{1}{n}\sum_{i=1}^{n}|(\hat{y}_i - y_i)| \tag{3.3}$$

Table 3 shows the error metrics calculated for both the model based on the SS-solver and the model based on MIKE+ for both areas of interest. P1 denotes priority area 1 and P2 denotes priority area 2.

| Validation metric [m] | SS P1 | MIKE+ P1 | SS P2 | MIKE+ P2 |
|---|---|---|---|---|
| RMSE (RTK) | 0.050 | 0.058 | 0.047 | 0.062 |
| RMSE (SWOT 456) | 0.077 | 0.097 | 0.17 | 0.15 |
| RMSE (SWOT 484) | 0.18 | 0.19 | - | - |
| MBE (RTK) | -0.019 | -0.018 | 0.013 | 0.010 |
| MBE (SWOT 456) | -0.024 | -0.029 | 0.040 | 0.036 |
| MBE (SWOT 484) | -0.17 | -0.18 | - | - |
| MAE (RTK) | 0.040 | 0.049 | 0.043 | 0.057 |
| MAE (SWOT 456) | 0.065 | 0.073 | 0.11 | 0.10 |
| MAE (SWOT 484) | 0.17 | 0.18 | - | - |

**Table 3:** Error metrics for SS-and MIKE+ models compared to ground truth RTK data and data from the SWOT mission.

Firstly, table 3 shows that for all error metrics the lowest values are found, when comparing the predicted WSE from the models to the ground truth RTK values. Furthermore, for all error metrics in priority area 1, the highest values are found, when comparing the predicted WSE from the models to the SWOT 484 dataset. Thereby, the models fit the SWOT 484 data, the least. For priority area 1, it can be seen that the RMSE is generally higher for the MIKE+ model compared to the SS model for both RTK and SWOT data. This difference could be due to the larger spatial increments used when setting up the MIKE+ model compared to the spatial increments in the SS-model. From table 3 it can be seen that the hydraulic models for area 1 all have a negative bias compared to the RTK measurements and SWOT datasets as all MBE values are negative. This implies that the model generally underestimates the WSE compared to the observed WSE values. For area 1, the MAE ranges from 4.0-17 cm for the SS model and 4.9-18 cm for the MIKE+ model.

As mentioned, the 484 SWOT dataset does not cover priority area 2. For priority area 2, it differs whether error metrics are lower for the SS model or the MIKE+ model. The RMSE ranges from 4.7-17 cm for the SS model and 6.2-15 cm for the MIKE+ model. The hydraulic models for area 2 all have a positive bias compared to the RTK measurements and SWOT dataset as all MBE values are positive. This implies that the models generally tend to overestimate the WSE compared to the observed WSE values. However, from figure 18 it can be seen that the SWOT 456 observations are not distributed randomly on each side of the models. Instead the SWOT 456 observations are located on the same side of the model along some sections, and thus there seem to be local bias at some sections along the chainage. This is especially the case for area 2, but it also seems to occur in some sections for area 1. The MAE ranges from 4.3-11 cm for the SS model and 5.7-10 cm for the MIKE+ model. Additionally,

the error metrics are generally lower for the models in priority area 1 compared to the error metrics for the models in priority area 2.

## 3.3 Övertorneå virtual station

Figure 20 shows the defined area of a virtual measuring station located upstream of Övertorneå together with the Sentinel-3 measurements used to create a river discharge time series. The Sentinel-3 observations shown on figure 20 are the observations that are left after sorting out observations in accordance to section 2.8.1.

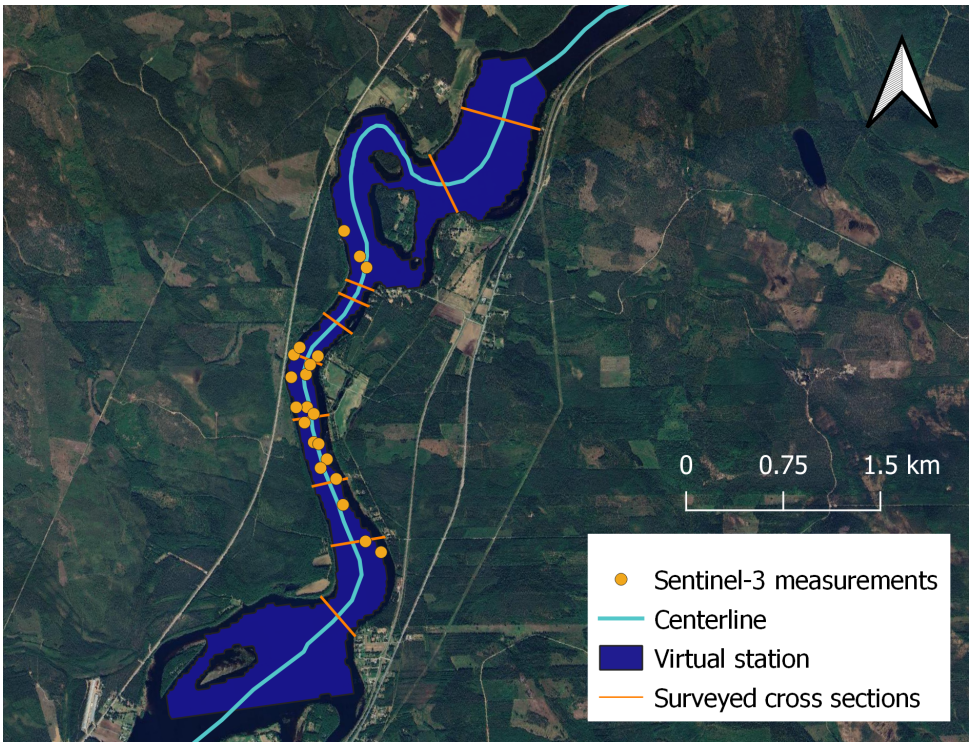


**Figure 20:** Sentinel-3 virtual station upstream of Övertorneå (EPSG:3006) and the Sentinel-3 measurements used to create discharge time series.

Based on the hydraulic model made with the SS-solver for area 1, rating curves have been constructed for each chainage point, where Sentinel-3 observations are obtained. Examples of the rating curves are shown in figure 21 at chainage points x=92950, x=94520 and x=95770. All 19 rating curves are shown in appendix 7.5.

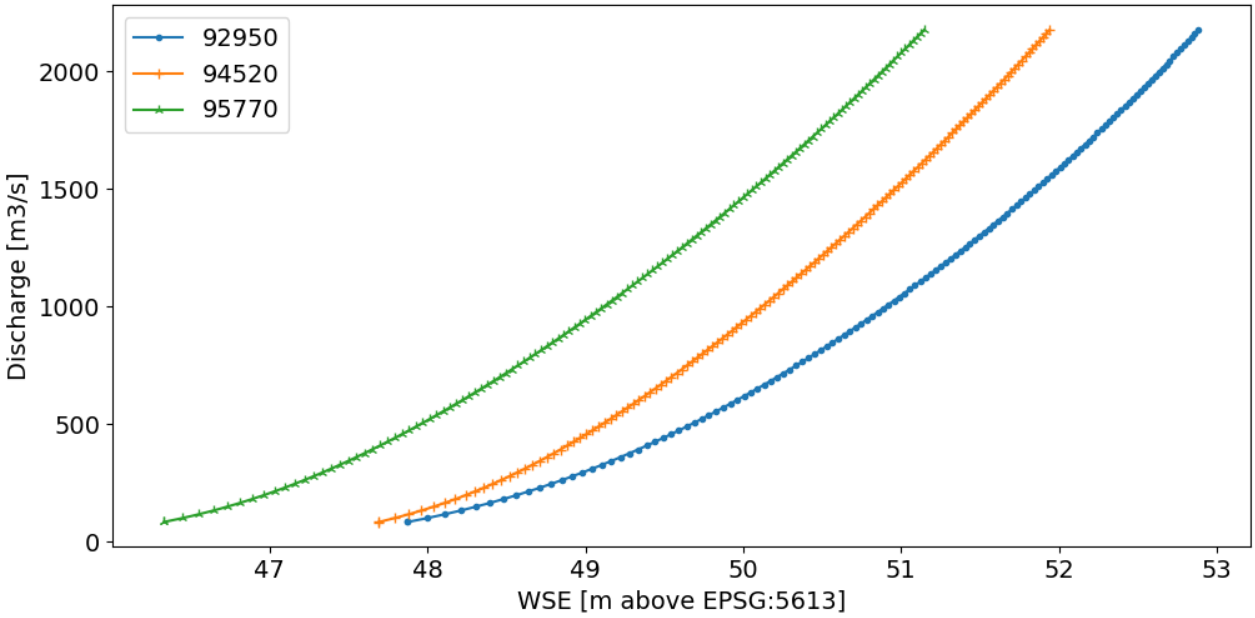


**Figure 21:** Rating curves at different chainage points within the virtual station made based on hydraulic model for area 1.

Higher chainage points are more dowstream on the river compared to lower chainage points. As the figure shows, the rating curves for the more upstream chainage points on the river are shifted to the right. Thus, the figure shows that the WSE is generally higher more upstream on the river at the same discharge values, which is as expected. A discharge time series is constructed based on the rating curves and Sentinel-3 observations. Figure 22 shows the river discharge time series (left) and a graph showing the predicted versus in-situ discharge at Pello (right).

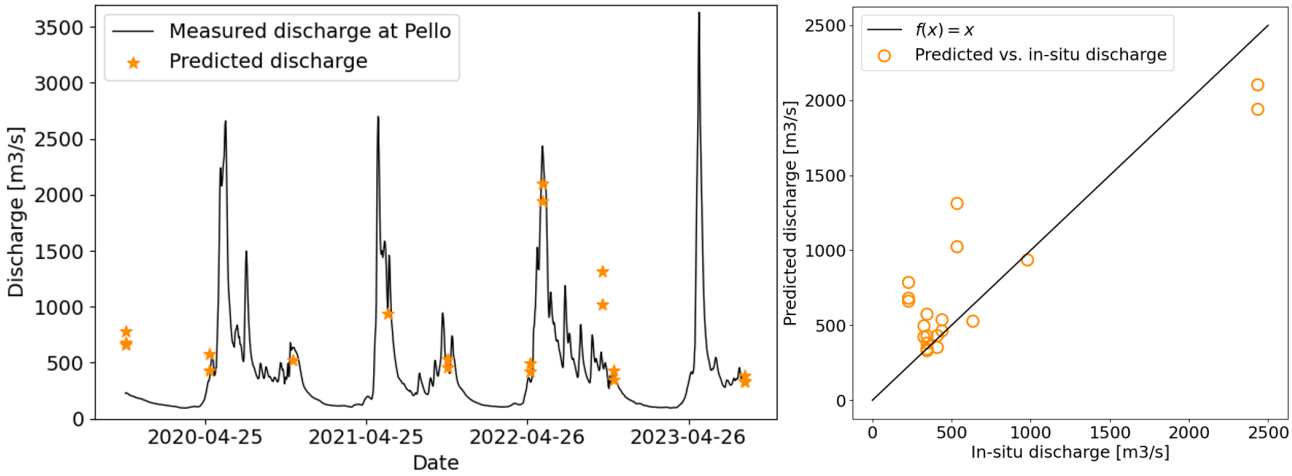


**Figure 22:** River discharge time series with predicted discharge at Övertorneå virtual station and measured discharge at Pello in-situ station (left). Predicted discharge versus in-situ discharge (right).

Figure 22 shows that the predicted discharge values at the virtual station are somewhat consistent with the measured in-situ discharge. However, the predicted discharges in late October in 2019 and mid October in 2022 are not consistent with the in-situ discharge. Additionally, the figure shows that predicted discharge for the same days differs, which is not as expected. It is likely due to, that the WSE is measured at different chainages and the discharge is thus predicted using different rating curves. When looking at the graph showing the predicted discharge versus in-situ discharge, it seems that the predicted discharge tends to be higher than the in-situ discharge except for high discharge observations.

## 3.4 Pello virtual station

Figure 23 shows the defined area of a virtual measuring station located downstream of Pello together with the Sentinel-3 measurements used to create a river discharge time series. The Sentinel-3 observations shown on figure 23 are the observations that are left after sorting out observations in accordance to section 2.8.1.

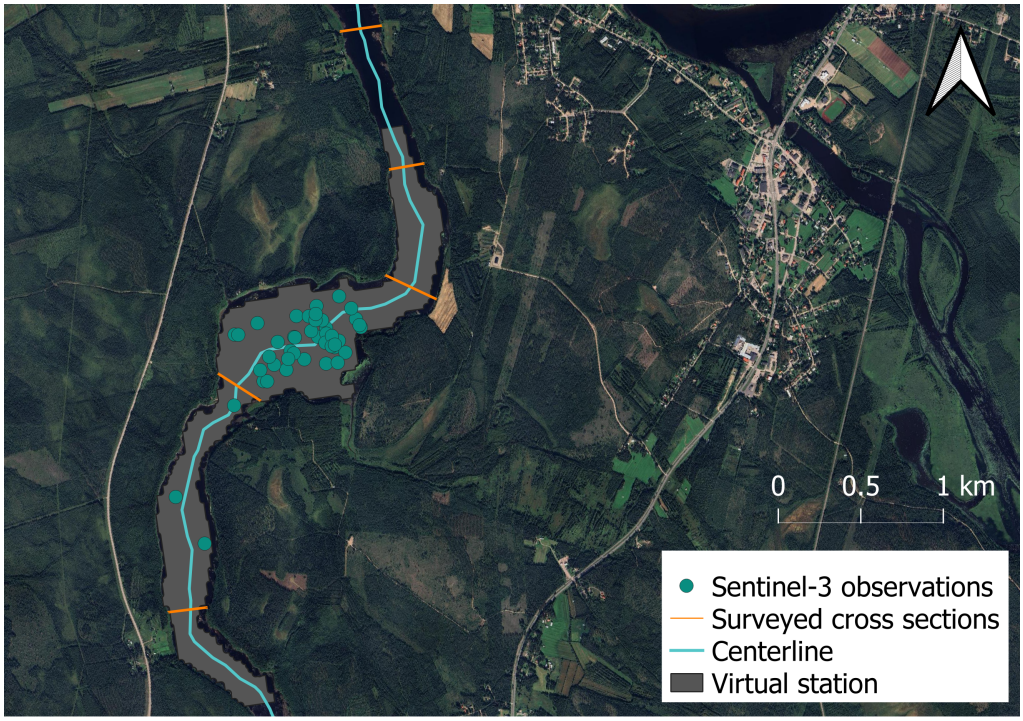


**Figure 23:** Sentinel-3 virtual station downstream of Pello (EPSG:3006) and the Sentinel-3 measurements used to create discharge time series.

Based on the hydraulic model made with the SS-solver for area 2, rating curves have been constructed for each chainage point, where Sentinel-3 observations are obtained. After sorting, 44 Sentinel-3 observations are left. The rating curves corresponding to the locations of the Sentinel-3 observations are shown in appendix 7.5. Based on these rating curves and

the Sentinel-3 observations, a discharge time series is constructed. Figure 23 shows the river discharge time series including both the predicted discharge and the in-situ discharge (left). Additionally, the right figure shows a comparison of the predicted discharge versus the in-situ discharge. Figure 24 shows that for the Pello virtual station the predicted discharge tends to be overestimated compared to the in-situ discharge.

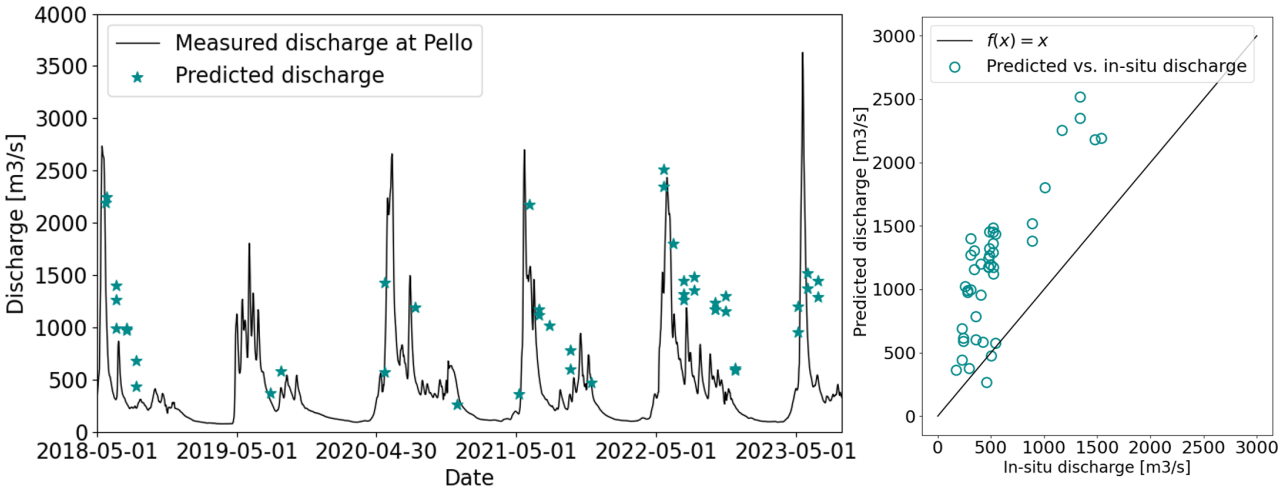


**Figure 24:** River discharge time series with predicted discharge at Pello virtual station and measured discharge at Pello in-situ station (left). Predicted discharge versus in-situ discharge (right).

Figure 24 shows that some of the predicted discharge values correlates well with the in-situ discharge. However, most of the predicted discharge values tends to be overestimated compared to the in-situ discharge. As for the Övertorneå vitual station, the predicted discharge for the same days differs, which is not as expected.

# 4 Discussion

As all results have been presented, the following sections will focus on discussing these results. First, the methods for obtaining data will be discussed. Hereafter, data gaps and the impact of these on the hydraulic models are discussed. Lastly, the model performance is discussed including the accuracy of the virtual station discharge time series.

## 4.1 Data from drone-borne WPR and the SWOT mission

Accurate cross-sectional geometry data is important when setting up hydraulic models for rivers, as the accuracy of the model predictions depends directly on the quality of the cross-sectional geometry data [2]. River bathymetry surveys can be made with an RTK GNSS receiver in rivers with shallow water. These surveys are costly, time consuming and often the

covered area is small compared to costs and time spent. Torne river is a large river, and some of the surveyed cross sections had widths up to 700 m [41]. In a river like Torne River, mapping the cross section bathymetry with a RTK GNSS receiver would be very time consuming and impossible in some sections due to large depths and high flow velocities. The survey time is reduced, when using drone-borne WPR to measure river bathymetry [3]. In the case of the Torne field site, up to 6 cross sections were surveyed per day. Other surveys were also conducted at each cross section. If WPR is the only survey method at each field site, the number of WPR surveyed cross sections could possibly be higher per day. Drone-borne WPR-measurements of bathymetry are limited to water bodies with electric conductivity less than 250 $\mu\mathrm{S/cm}$. At the field sites the electric conductivity ranged from 26-37 $\mu\mathrm{S/cm}$ (see appendix 7.6), which is below the maximum electric conductivity, where the WPR-payload can be used. Additionally, a flight altitude of maximum 0.5 m is recommended for the drone-borne WPR to decrease the noise level of the data. At the Torne River field survey the low-altitude flights following the water surface showed to work without problems [41]. Thus, the drone-borne WPR showed to be an efficient method for mapping the bathymetry of the Torne River. One disadvantage of the of mapping bathymetry with drone-borne WPR, is that post processing efforts of WPR datasets are higher than for other methods that maps river bathymetry (e.g. sonar/echo sounder datasets) [42].

The WSE collected by the SWOT satellite has a spatial resolution of 50 m and a height accuracy of 10 cm. It has been found that for rivers with a width of less than 200 m, no pixel might fully represent the WSE (due to the influence of banks). Additionally, larger uncertainties for pixels are present near river banks and islands [19]. The SWOT data can be used for the Torne River as the river is wide, but it might not be applicable for smaller rivers. In this project, the SWOT 456 dataset from September 5th 2024 and the SWOT 484 dataset from September 6th are used. The SWOT 456 dataset was used to calibrate the Manning numbers with along the river as this dataset was consistent with the ground truth RTK GNSS observations. Priority area 1 is covered by both SWOT datasets, while priority area 2 is only covered by the SWOT 456 dataset. From figure 16 it is clear that there is a difference between the two SWOT datasets measured on different days. The WSE measured on September 6th (484) is generally higher than the WSE measured on September 5th (456). The difference in SWOT-data does not correlate with the measured discharge at the in-situ station at Pello, which is noticeable. On September 5th, the discharge measured at the Pello station was 306.9 $m^3/s$, while it was 301.7 $m^3/s$ on September 6th. It would be expected that a higher discharge would yield a higher WSE, and thus the difference in the SWOT datasets might be caused by other factors. As the height accuracy is 10 cm, this could be a possible reason for the difference in the two datasets.

## 4.2 Data gaps

At the survey sites UAS-borne WPR has been used to measure the river bathymetry, and the bank elevation has been derived from the Finnish DEM for the left side of the river and the GLO-30 DEM for the right side of the river. The combination of datasets for some cross sections result in datagaps between the WPR data and DEM data. Cross-sections with data gaps present a larger uncertainty compared to cross sections without data gaps, as the geometry of the cross sections in the data gaps are unknown. In this project, the data gaps have been handled by making linear interpolation between WPR and DEM data. This affects the cross sectional area and the wetted perimeter, and thus the relationships between cross sectional area and WSE as well as the relationship between hydraulic radius and WSE. It is among other these relationships that are used, when calculating the WSE along the river both with the SS-solver and with MIKE+. A cross sectional area that is too small compared to the actual cross sectional area, can result in that the WSE is higher compared to the actual WSE for a certain discharge (as the water is "forced" through a smaller area). If the cross sectional area on the other hand is larger than the actual cross sectional area, the computed WSE might be lower than the actual WSE. Ideally the data gaps are prevented to get the most accurate cross sections. A way to prevent data gaps, would be conduct the drone-borne WPR measurements on days with high flow. Additionally, the data used to construct the DEM's should be conducted on days with low flow. This approach would result in that elevation data from the submerged part of the river would overlap with the elevation data from the riverbanks.

In figure 16 that shows the hydraulic models, SWOT and ground truth data for priority area 1, it can be seen that for some sections of the river, there gaps where no SWOT or ground truth data is present. Such a datagap is seen between x = 91400 and x = 93400 on figure 16. In data gaps like these, the simulated WSE from the hydraulic models might be quite inaccurate compared to the actual WSE. For example the water surface slope could be steeper, possibly creating a section with super-critical flow conditions. However, this remains unknown as no data is available for this area. For priority area 2 the 456 SWOT data is available for the whole area, and thus there are no data gaps presents in the same order as for priority area 1.

## 4.3 Model performance

Different simplifications have been used to set up the hydraulic models. Steady state is assumed when setting up the hydraulic models using both the SS-solver and the MIKE+ software, which is a simplification of the actual flow conditions. Additionally, the assumption of no lateral inflow is also a simplification compared to the actual conditions. These simplifications might affect the accuracy of the hydraulic models. However, as the calibrated models are consistent with both the SWOT data and ground truth data, they are assumed to be reliable

for the intended application.

When calculating the boundary conditions, the following assumptions are made: uniform flow downstream of the last cross section in each priority area, the downstream cross-sectional geometry is identical to the geometry of the most downstream cross section, and the downstream bed slope is calculated and calibrated based on the upstream slope. The downstream bed slope will however only affect the most downstream cross section [5]. The downstream WSE boundary condition affects the hydraulic models. A boundary condition that is too high will for example result in a higher WSE upstream of the boundary condition with the largest effect close to the boundary condition. The Manning $n$ and downstream bed slope used to calculate the boundary conditions has been calibrated against the most downstream ground truth WSE measurement by trial and error.

The Froude numbers have been calculated at all chainage points along the river for both areas and both hydraulic models. These showed the same pattern, but that the Froude numbers calculated in MIKE+ were generally higher than the Froude numbers calculated using the SS-solver. The reason for this is that the Froude numbers are calculated differently, when using the SS-solver and MIKE+. When using the SS-solver, the Froude numbers are calculated using equation 2.2, where the depth (*w*) is the flow depth at a distance along the reference line equal to zero. At a distance along the reference line equal to zero, a flow depth close to the maximum depth is found for most cross sections. This might result in a depth, which yields a too small Froude number. In MIKE+ the Froude numbers are calculated using the following equation [43]:

$$\mathrm{Fr} = \frac{Q}{A \cdot \sqrt{g \cdot \frac{A}{b_s}}} = \frac{v}{\sqrt{g \cdot \frac{A}{b_s}}} \tag{4.1}$$

The difference from equation 2.2 is that the flow depth is replaced with a term, where the cross sectional area (*A*) is divided by the channel width at surface ($b_s$). Thereby, the average depth of the channel is taken into account, when calculating the Froude number in MIKE+. As the term $\frac{A}{b_s}$ is the average depth, the resulting Froude number will be higher compared to Froude numbers calculated using the maximum depth. In continuation of this, the Froude numbers calculated in MIKE+ are more reliable as the overall geometry of the channel is considered.

However, for both models in both areas the Froude numbers are below one and ranges from 0.025 to 0.31 at a discharge of 300.5 $m^3/s$. This indicates that with the available data used to set up the models, the hydraulic model created with the SS-solver is reliable as the flow is not super-critical at any point along the river. The SS-solver is initialized with a downstream boundary and then calculates the WSE moving upwards along the chainage in stepwise increments. For sections with super-critical flow, the WSE must on the other hand be computed starting upstream in the section and moving downstream. Additionally, it has been tested whether a higher discharge would result in Froude numbers that exceeds one. Both models

for both areas have been run with a discharge of 2000 $m^3/s$, which did not result in Froude numbers above 1. Even though, the Froude numbers does not exceed 1 with the available data, some sections of the river might be super-critical in reality at a certain discharge range. The reason for this can be that not enough data is available. When looking at figure 16 and 18 it can be seen that no field sites have been placed on the steep part of the river. Thus, data is generally missing on the steeper sections on the river, where super-critical flow is more likely to occur. The cross-sectional geometry may differ a lot from the interpolated geometry of surrounding cross-sections, which can affect the Froude numbers. Furthermore there might be overfalls in the river, where the riverbed elevation might be higher just before the overfall. This would result in an even steeper bed slope, which might also lead to super critical flow. However, as data for these sections are missing, this is uncertain.

### 4.3.1 Calibration of the bed roughness

The bed roughness at different sections of the river has been calibrated against the SWOT 456 observations of the WSE by trial and error using the SS-solver. This yielded Manning numbers (Manning *n*) for the different sections between 0.023-0.10 $s/m^{1/3}$ for priority area 1, and 0.03-0.16 $s/m^{1/3}$ for priority area 2. The Manning $n$ for river sections that are regular and without boulders and courser grains is typically in the range of 0.025-0.60. The Manning $n$ for river sections that are irregular and more rough, is typically in the range of 0.035-0.10 [33]. Two of the calibrated Manning numbers are respectively lower and higher than this (0.023 $s/m^{1/3}$ and 0.16 $s/m^{1/3}$). Some of the factors that can affect the Manning number are: surface roughness, vegetation, and channel irregularity. Coarser grains, presence of vegetation and channel irregularities all increase the roughness factor, and thus Manning numbers outside the typical range for rivers are possible [33].

The calibrated Manning numbers might present an uncertainty in terms of the model application of a virtual station. The reason for this is that the Manning number is affected by the discharge-WSE relationship. If the discharge an WSE increases the Manning number likely decreases as the irregularities of the river bed becomes less influencing of the Manning $n$ [33]. This increases the uncertainty of the rating curves constructed for the virtual stations.

### 4.3.2 Model improvements

One way to improve the hydraulic models would be to collect more bathymetry data. Bathymetry data for the steeper sections of the river would especially be valuable, because super-critical flow conditions are more likely to happen here. The SWOT mission could be a valuable tool for planning and deciding the placements of the field sites along the river. The SWOT data can give an indication of which parts of the river are steep and which are flat. Then some field

sites can be placed on the steep sections and some on the flat sections. Additionally, it would be preferable to place the field sites on sections on the river where no SWOT data is available to avoid WSE observation data gaps along the river. However, the access to the cross sections does still need to be considered.

With the available data, another way to improve the models, would be to construct more cross sections along the river by using DEM's. The river bank elevations can be retrieved from the DEM's and the submerged parts of the river can be assumed to have a certain shape. Additionally, it could be considered to use a distribution of different Manning numbers along the cross section. This could be considered as large boulders are often collected at the bottom of the river, which results in a larger roughness there compared to the river banks [33]. It is possible to make a distributed roughness in MIKE+ [37].

### 4.3.3 Övertorneå virtual station

At the Övertorneå virtual station, the calibrated hydraulic model based on the SS-solver for area 1 has been used to create discharge-WSE relationships (rating curves) at the chainage points of the Sentinel-3 observations. From the rating curves, the corresponding discharges of the Sentinel-3 WSE observations, have been derived and compared to the in-situ discharges measured by the Pello station. Most of the predicted discharge values are reasonably close to the in-situ discharge. However, some of the predicted discharges are over 500 $m^3/s$ higher than the in-situ discharge. As figure 22 among other showed, the predicted discharges in late October in 2019 and mid October in 2022 are not consistent with the in-situ discharge. When the river is frozen, it will result in the Sentinel-3 satellite measuring the elevation of the ice (and snow). This will result in an observation of elevation that higher than the actual WSE of the flowing water [31]. The weather in Lapland can vary in October, and is often above the freezing point in the day but below at night [44]. As the temperature varies, it also varies whether the Torne River is frozen or not in October. An explanation for the high predicted discharges in late October in 2019 and mid October in 2022, could therefore be that the river was frozen on these dates. However, a Sentinel-3 observation has also been made in late October of 2021. This observation is close to the in-situ discharge, which is why the observations in October har not sorted out. The air temperature were as follows on the days of the Sentinel-3 observations in October: -13 to -7 °C on October 28th 2019, -2 to 0 °C on October 26th 2021, and 0 to 6 °C on October 12th 2022 [45]. Thus, the observations in October of 2019 and 2021, fits with the hypothesis of a frozen river. However, the air temperature on October 12th 2022 is above the freezing point (0-6 °C), and it is unlikely that the river is frozen in this temperature. On this date, the predicted discharge is more than 500 $m^3/s$ higher than the in-situ discharge. Thus, the frozen river hypothesis does not seem to be valid for this date, and other factors might responsible for the difference.

Additionally, figure 22 shows that predicted discharge for the same days differs, which is not as expected. It is likely due to, that the WSE is measured at different chainages and the discharge is thus predicted using different rating curves. This could be due to that the rating curves made at chainage points closer to the survey sites are more correct. This is possible because the cross-sectional geometry data at these sites is more accurate than the interpolated cross-sectional geometry between survey sites. Another reason could be that the along-track resolution of the Sentinel-3 mission is 300 m [39, 6], which at low discharge is more than the width of some of the narrow sections of the river in the virtual station. As seen on figure 20 most of the Sentinel-3 observations are located in the narrow part of the area of the virtual station. This could possibly affect the Sentinel-3 observations. Solutions for this could be to choose another location for the virtual station that is wider or to retrieve WSE observations from satellite mission with larger spatial resolution (e.g. ICESat-2 [6]).

### 4.3.4 Pello virtual station

At the Pello virtual station, the calibrated hydraulic model based on the SS-solver for area 2 has been used to create discharge-WSE relationships (rating curves) at the chainage points of the Sentinel-3 observations. Figure 24 shows that for the Pello virtual station some of the predicted discharge values correlates well with the in-situ discharge. However, most of the predicted discharge values tends to be remarkably overestimated compared to the in-situ discharge. The Pello virtual station is located between chainage x=55110-59670, where most of the Sentinel-3 observations are located within a chainage of x = 56500-57330. On figure 18 it can be seen that within the chainage, where most Sentinel-3 observations are located, both hydraulic models tends to underestimate the WSE compared to the SWOT 456 observations. This could be an explanation for the overestimation of discharge. If the model underestimates the WSE at a given discharge, then the discharge is overestimated compared to the WSE when constructing rating curves for these chainage points. When the Sentinel-3 observations are then used to retrieve the corresponding discharge using the discharge-WSE relationships (rating curves), the retrieved discharges will be higher than the actual discharges. It can additionally be seen in figure 24 that the predicted discharge values seem to have peaks on the same days, where discharge peaks have been observed in-situ. However, the predicted discharges are generally higher than the in-situ discharges.

The reason for the underestimation of the WSE by the hydraulic models within the location of most of the Sentinel-3 observations, could be due to that an overfall occurs around XS23. When looking at figure 23 it seems that a large lake or pool is situated in the middle of the river, where most of the Sentinel-3 observations are located. Furthermore, it is shown on figure 18 that the section of the river after XS23 has a steep water surface. Therefore it is likely that an overfall occurs here. As mentioned in section 2.6, it is the location and shape of

the cross section at the control section of an overfall that determines the WSE. When looking at figure 18 is seems that the surveyed cross section (blue triangle at x = 57400) at the overfall is located a bit downstream of the control section for the overfall. This can be seen, when comparing the surveyed cross section with the SWOT 456 observations. If the surveyed cross section is not located close enough to the location of the control section, it can result in that the WSE is not calculated correctly. In continuation of this, if the surveyed cross section has a lower elevation than the actual control section, the simulated WSE will be underestimated both upstream of and at the overfall. In this case, a solution could be to make a virtual cross section that is identical to XS23, but elevated and located at the control section (i.e. more upstream on the river). This could result in a more accurate hydraulic model for priority area 2 and thus a more accurate virtual station at Pello.

# 5 Conclusion

The purpose of this project was to use UAS hydrometry surveys and WSE observations from the SWOT mission instead of traditional in situ measurements to model the WSE along the Torne River. Firstly, it can be concluded that UAS-borne WPR is an efficient method for mapping river bathymetry compared to traditional in-situ methods. The WPR data of the submerged parts of the river contribute to accurate information about the cross-sectional geometry of rivers, which is important when setting up hydraulic models for rivers.

For each priority area, two hydraulic models have been set up; one using a SS-solver and one using the MIKE+ software. For both priority areas, it can be concluded that the hydraulic model results computed using the SS-solver are nearly identical to those obtained with the MIKE+ software. The Manning numbers along the river have been calibrated against SWOT 456 satellite observations, yielding Manning numbers of 0.023-0.10 $s/m^{1/3}$ for area 1, and 0.030-0.16 $s/m^{1/3}$ for area 2. In continuation of this, it can be concluded that the hydraulic models correlate with both SWOT observations and ground truth RTK observations. Negative MBE values for the hydraulic models for priority area 1 compared to ground truth and SWOT observations, implies that the models tend to underestimate the WSE compared to the observed WSE. The opposite is the case for priority area 2. However, especially for the models in area 2, the models seem to have local biases as the SWOT 456 observations are not distributed randomly on each side of the models.

The Froude numbers were below 1 along the chainage for both models in both areas for a discharge of 300.5 m3/s. However, a difference between the Froude numbers computed with the SS-solver and MIKE+ were observed, which were due to different calculation methods. Even though, the Froude numbers does not exceed 1 with the available data, some sections of the river might be super-critical in reality at a given discharge. Data is generally missing on the steeper sections on the river, where super-critical flow is more likely to occur. The cross-sectional geometry may differ a lot from the interpolated geometry of surrounding cross-sections, which can affect the Froude numbers. In relation to this, the SWOT mission could be a valuable tool for deciding the placements of the field sites along rivers to cover both steep an flat river sections.

Lastly, the project investigated the possibilities of developing virtual stations on the Torne River, and found that with the available data, the Övertorneå virtual station predicts the discharge more accurately than the Pello virtual station. This is a result of the hydraulic model for area 1 being more accurate than the hydraulic model for area 2, as more cross sectional data was available within the area of Övertorneå virtual station than within the area Pello virtual station. At the Pello virtual station the predicted discharge was clearly overestimated, which is likely due to the presence of an overfall in the downstream end of the virtual station.

# 6 References

# References


[1] Henrik Grosen. *Deliverable 3.1: WSE Surveying Protocol*. Tech. rep. Unmanned Airborne Water Observing System, 2024.

[2] S. Grimaldi et al. "Effective Representation of River Geometry in Hydraulic Flood Forecast Models". In: *Water Resources Research* 54.2 (2018), pp. 1031–1057. DOI: https://doi.org/10.1002/2017WR021765. URL: https://agupubs.onlinelibrary.wiley.com/doi/abs/10.1002/2017WR021765.

[3] Filippo Bandini et al. "Mapping inland water bathymetry with Ground Penetrating Radar (GPR) on board Unmanned Aerial Systems (UASs)". In: *Journal of Hydrology* 616 (2023), p. 128789. ISSN: 0022-1694. DOI: https://doi.org/10.1016/j.jhydrol.2022.128789. URL: https://www.sciencedirect.com/science/article/pii/S0022169422013592.

[4] UAWOS. *UNMANNED AIRBORNE WATER OBSERVING SYSTEM*. 2024. URL: https://uawos.dtu.dk/. (accessed: 01.10.2024).

[5] Cécile M. M. Kittel et al. "Hydraulic model calibration using CryoSat-2 observations in the Zambezi catchment". English. In: *Water Resources Research* 57.9 (2021). ISSN: 0043-1397. DOI: 10.1029/2020WR029261.

[6] Monica Coppo Frias et al. "River hydraulic modeling with ICESat-2 land and water surface elevation". eng. In: *Hydrology and Earth System Sciences* 27.5 (2023), pp. 1011–1032. ISSN: 16077938, 10275606. DOI: 10.5194/hess-27-1011-2023.

[7] Åsa Davidsson. *Utredning av versvämning i Norrbottens län 2023*. Tech. rep. Länsstyrelsen Norrbotten, 2023.

[8] SMHI. *Sveriges största vattendrag*. URL: https://www.smhi.se/kunskapsbanken/hydrologi/sveriges-vattendrag/sveriges-storsta-vattendrag-1.167648. (accessed: 03.09.2024).

[9] VESI.fi. *WATERINFO.fi*. URL: https://www.vesi.fi/en/karttapalvelu/. (accessed: 19.09.2024).

[10] Lantmäteriet. *Reference Systems*. URL: https://www.lantmateriet.se/en/geodata/gps-geodesi-och-swepos/reference-systems/#anchor-0. (accessed: 12.11.2024).

[11] VirtualSurveyor. *What is an EPSG Code?* 2024. URL: https://support.virtual-surveyor.com/support/solutions/articles/1000261353-what-is-an-epsg-code-. (accessed: 23.11.2024).

[12] MapTiler Team. *Coordinate Systems Worldwide*. 2024. URL: https://epsg.io/. (accessed: 23.11.2024).

[13] Propeller. *What Are Ellipsoid and Geoid Heights?* URL: https://help.propelleraero.com/hc/en-us/articles/19383617598743-What-Are-Ellipsoid-and-Geoid-Heights. (accessed: 12.11.2024).

[14] DJI enterprise. *Geoid vs Ellipsoid: What's the Difference and Why Does it Matter?* URL: https://enterprise-insights.dji.com/blog/geoid-vs-ellipsoid. (accessed: 12.11.2024).

[15] Daniel O'Donohue. *What is GNSS RTK*. URL: https://mapscaping.com/what-is-gnss-rtk/. (accessed: 13.09.2024).

[16] NASA Jet Propulsion Laboratory. *Surface Water and Ocean topography*. URL: https://swot.jpl.nasa.gov/. (accessed: 16.09.2024).

[17] Joseph M. Smith. *NASA's Surface Water and Ocean Topography (SWOT) Mission Data Release*. URL: https://www.earthdata.nasa.gov/learn/articles/swot-data-release. (accessed: 16.09.2024).

[18] Steven P. Neeck et al. "Surface Water and Ocean Topography (SWOT) mission". In: *Sensors, Systems, and Next-Generation Satellites XVI*. Ed. by Roland Meynart, Steven P. Neeck, and Haruhisa Shimoda. Vol. 8533. SPIE, 2012, 85330G. DOI: 10.1117/12.981151. URL: https://doi.org/10.1117/12.981151.

[19] Kevin Oberg (Oberg Hydroacoustics). NIHW2024, Mini-Workshop; Hydrometry using satellite and drones. Sept. 24, 2024.

[20] Peter Fitzgibbon. *SWOT gets ready for launch*. 2022. URL: https://www.geoconnexion.com/in-depth/swot-gets-ready-for-launch. (accessed: 16.09.2024).

[21] NASA Earth Data. *NASA Earth Data Search*. 2024. URL: https://search.earthdata.nasa.gov/search?fpj=SWOT. (accessed: 17.09.2024).

[22] David J. Daniels. *Ground penetrating radar-2nd edition*. IEE, 2004, pp. xiv+726. DOI: 10.1049/PBRA015E.

[23] Angelica Tarpanelli et al. *Deliverable 4.1: Technical Report on Rating Curve estimation using UAS hydrometry*. Tech. rep. Version 4. Unmanned Airborne Water Observing System, UAWOS, 2024.

[24] Radar Systems Inc. *Zond Aero 500 GPR*. 2024. URL: https://www.radsys.lv/en/index/. (accessed: 01.10.2024).

[25] Alexey Kadek et al. *Deliverable 2.2: Water Penetrating Radar Payload*. Tech. rep. Version 3. Unmanned Airborne Water Observing System, UAWOS, 2023.

[26] Kent Ohlsson (Geodetist at Lantmäteriet). NIHW2024, Mini-Workshop; Precision in height measurements with levelling and GNSS - Introduction. Sept. 24, 2024.

[27] UAWOS. *Water Penetrating Radar*. 2024. URL: https://uawos.dtu.dk/payloads/water-penetrating-radar. (accessed: 01.10.2024).

[28] Cyrus G. Malmberg and Arthur A. Maryott. "Dielectric constant of water from 0 to 100 C". In: *Journal of research of the National Bureau of Standards* 56 (1956), p. 1. URL: https://api.semanticscholar.org/CorpusID:96483241.

[29] COPERNICUS Contributing Missions Online. *Copernicus DEM - Global and European Digital Elevation Model (COP-DEM)*. 2022. URL: https://spacedata.copernicus.eu/collections/copernicus-digital-elevation-modelr. (accessed: 11.10.2024).

[30] NSL National Land Survey of Finland. *Elevation model 2 m*. URL: https://www.maanmittauslaitos.fi/en/maps-and-spatial-data/datasets-and-interfaces/product-descriptions/elevation-model-2-m. (accessed: 11.10.2024).

[31] Peter Bauer-Gottwein. Personal Communication. 2024.

[32] Ven Te Chow. "Open-channel hydraulics". In: McGraw-Hill Book Company, Inc., 1959. Chap. Chapter 1 - Open-channel flow and its classifications.

[33] Ven Te Chow. "Open-channel hydraulics". In: McGraw-Hill Book Company, Inc., 1959. Chap. Chapter 5 - Development of uniform flow and its formulas.

[34] Peter Bauer-Gottwein. *River Routing - Lecture Notes*. 12320 Hydrology - Spring 2024 Edition.

[35] Ven Te Chow. "Open-channel hydraulics". In: McGraw-Hill Book Company, Inc., 1959. Chap. Chapter 3 - Energy and momentum principles.

[36] Ven Te Chow. "Open-channel hydraulics". In: McGraw-Hill Book Company, Inc., 1959. Chap. Chapter 4 - Critical flow: its computation and applications.

[37] DHI A/S. *MIKE 1D - DHI Simulation Engine for 1D river and urban modelling Reference Manual*. 2022.

[38] Peter Bauer-Gottwein et al. "Hydraulics of Time-Variable Water Surface Slope in Rivers Observed by Satellite Altimetry". In: *Remote Sensing* 16.21 (2024). ISSN: 2072-4292. DOI: 10.3390/rs16214010. URL: https://www.mdpi.com/2072-4292/16/21/4010.

[39] European Space Agency. *S3 Mission*. URL: https://sentiwiki.copernicus.eu/web/s3-mission#S3Mission-SatelliteDescriptionS3-Mission-Satellite-Descriptiontrue. (accessed: 21.11.2024).

[40] Muniraj Sahihya Padhma. *A Comprehensive Introduction to Evaluating Regression Models*. 2024. URL: https://www.analyticsvidhya.com/blog/2021/10/evaluation-metric-for-regression-models/. (accessed: 10.11.2024).

[41] UAWOS. *Torne_survey*. 2024. URL: https://uawos.dtu.dk/news-and-events/torne_survey. (accessed: 24.11.2024).

[42] Henrik Grosen, Sune Nielsen, and Peter Bauer-Gottwein. *Deliverable 3.2: Riverbed Geometry Surveying Protocol*. Tech. rep. Version 3. Unmanned Airborne Water Observing System, UAWOS, 2024.

[43] DHI A/S. *MIKE 11 - A modelling system for Rivers and Channels User Guide*. 2011.

[44] Weather & Climate. *Pello weather in October (Lapland, Finland)*. URL: https://weather-and-climate.com/pello-lapland-fi-October-averages. (accessed: 22.11.2024).

[45] timeanddate. *Past Weather in Pello, Finland*. URL: https://www.timeanddate.com/weather/@642368/historic?month=10&year=2022. (accessed: 22.11.2024).

[46] Neil M. Rotta et al. "A comprehensive analysis of operations and mass flows in postharvest processing of washed coffee". In: *Resources, Conservation and Recycling* 170 (2021), p. 105554. ISSN: 0921-3449. URL: https://www.sciencedirect.com/science/article/pii/S0921344921001610.

[47] NASA Earth Data. *Ka-band Radar Interferometer (KaRIn)*. URL: https://www.earthdata.nasa.gov/sensors/karin. (accessed: 16.09.2024).

# 7 Appendix

## 7.1 Overview of the area of interest

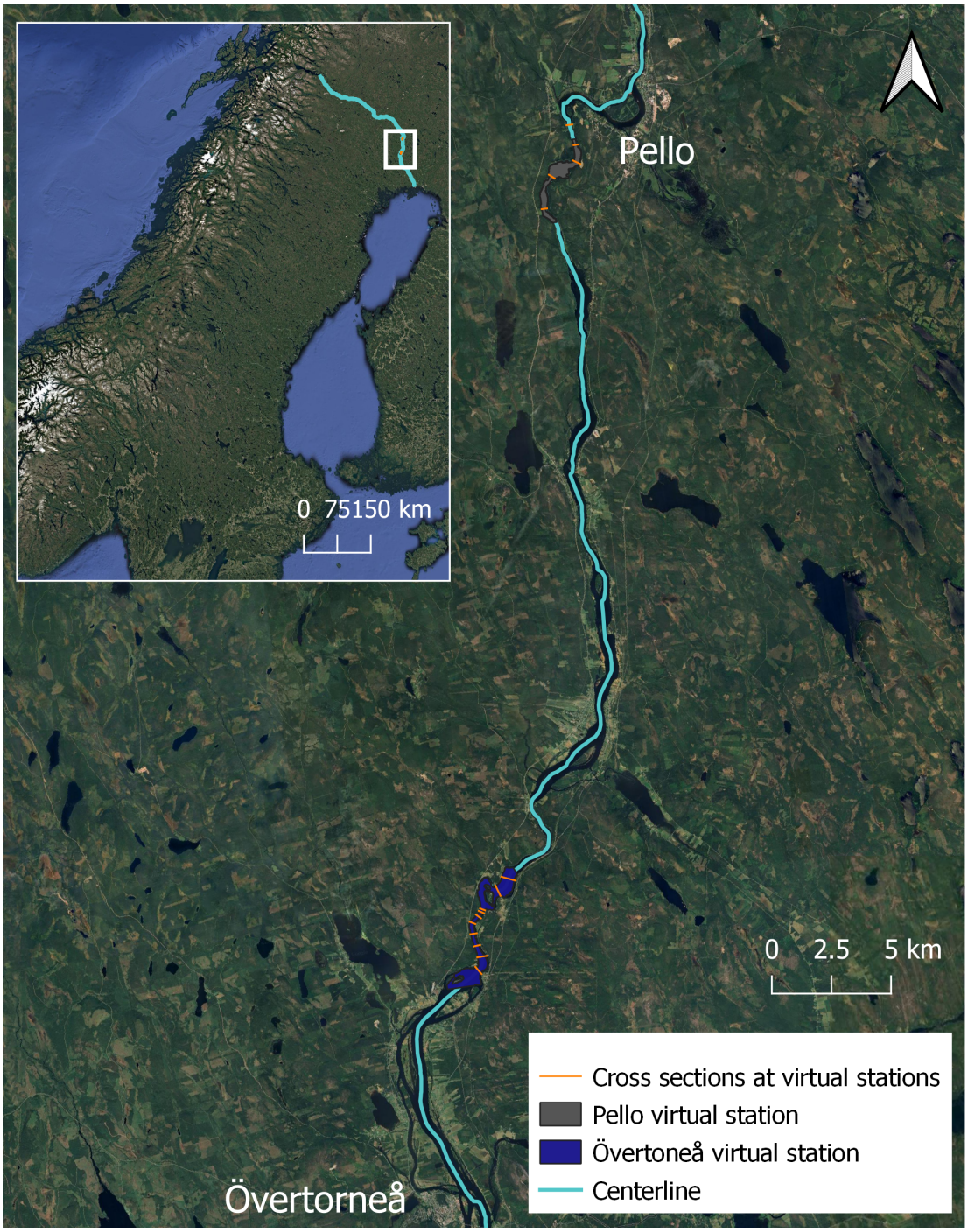


**Figure 25:** Overview of the area of interest including the two virtual stations and surveyed cross sections located within the virtual stations (EPSG:3006). The Pello virtual station is located within priority area 2 and the Övertorneå virtual station is located within priority area 1.

## 7.2 Boundary condition

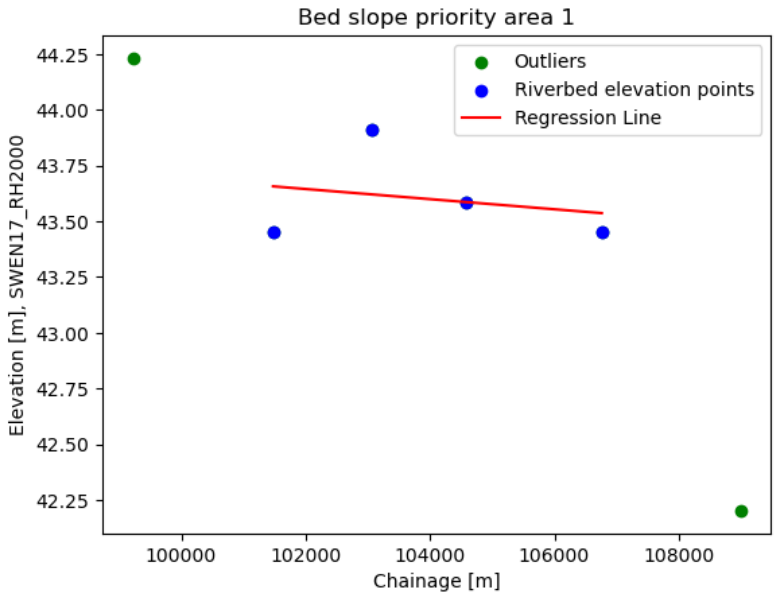


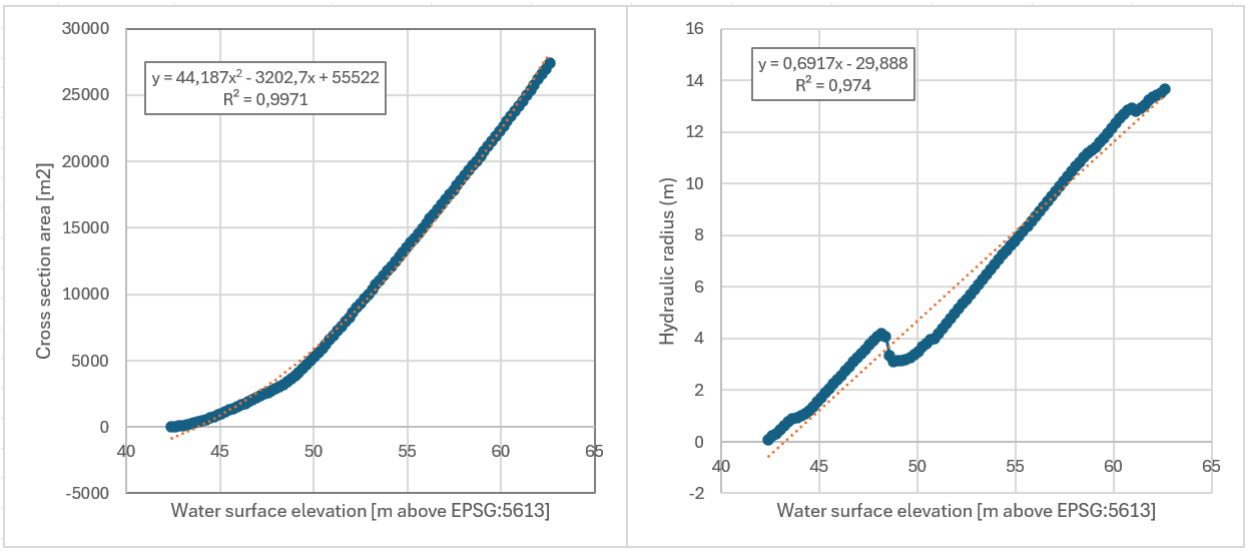


**Figure 26:** Relationship between cross sectional area and WSE for area 1 (XS19) (left). Relationship between hydraulic radius and WSE for area 1 (XS19) (right).

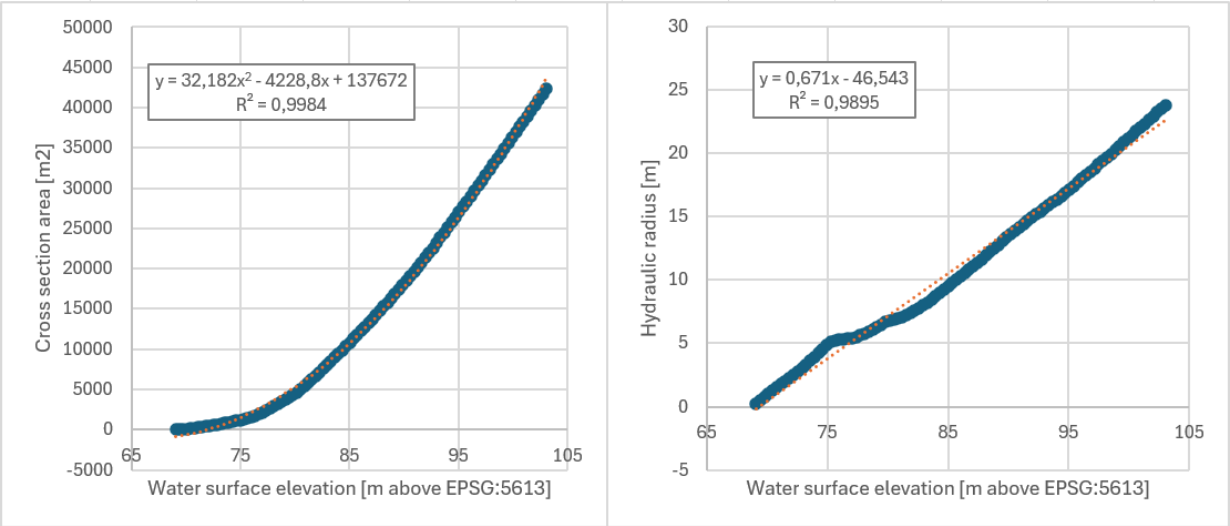


**Figure 27:** Relationship between cross sectional area and WSE for area 2 (XS24) (left). Relationship between hydraulic radius and WSE for area 2 (XS24) (right).

## 7.3 WSE measurements with RTK GNSS reciever

| **Survey site** | **WSE in situ average (m, SWEN17_RH2000)** |
|---|---|
| XS1 | 50.06 |
| XS2 | 50.04 |
| XS3 | 48.90 |
| XS4 | 48.76 |
| XS5 | 48.47 |
| XS6 | 47.56 |
| XS7 | 47.42 |
| XS8 | 46.87 |
| XS9 | 46.60 |
| XS10 | 46.44 |
| XS12 | 46.23 |
| XS14 | 46.19 |
| XS17 | 46.04 |
| XS19 | 45.95 |
| XS20 | 76.16 |
| XS21 | 75.85 |
| XS22 | 75.83 |
| XS24 | 72.00 |

**Table 1:** WSE measured by RTK GNSS receiver.

## 7.4 Results of level 4 processing of cross sections

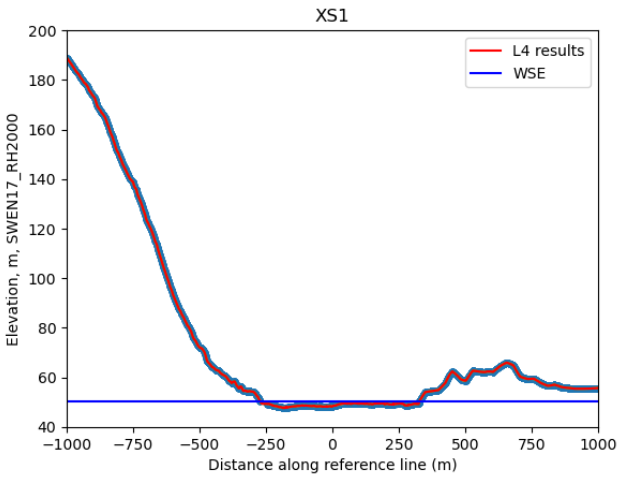


**Figure 28:** XS1

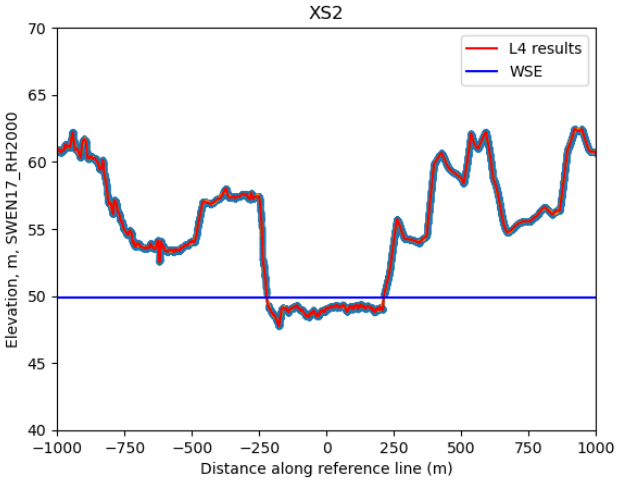


**Figure 29:** XS2

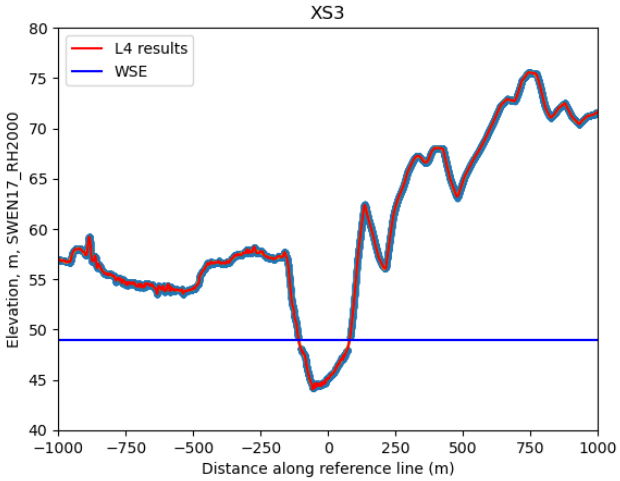


**Figure 30:** XS3

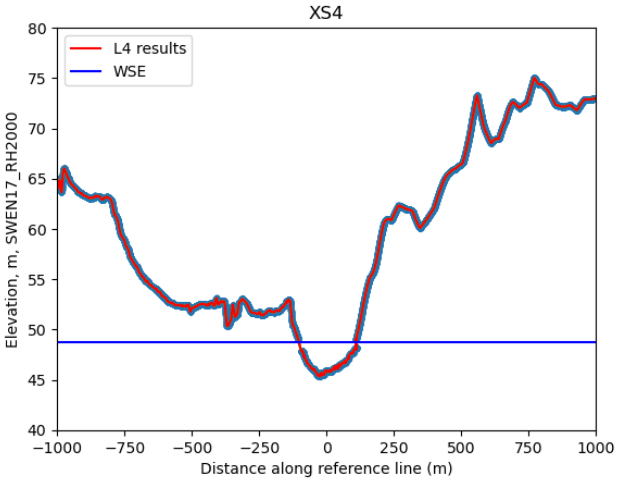


**Figure 31:** XS4

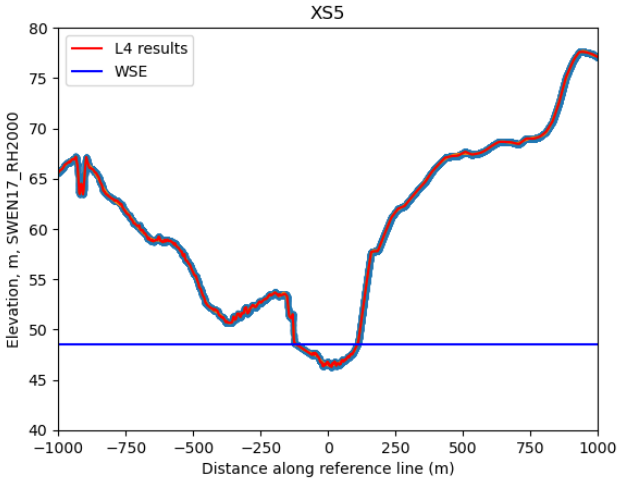


**Figure 32:** XS5

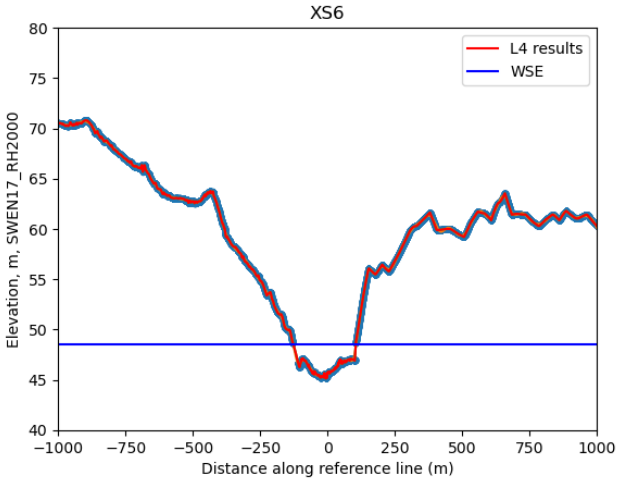


**Figure 33:** XS6

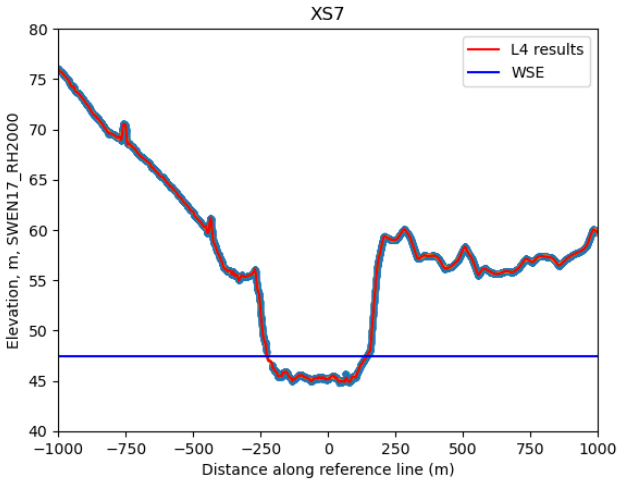


**Figure 34:** XS7

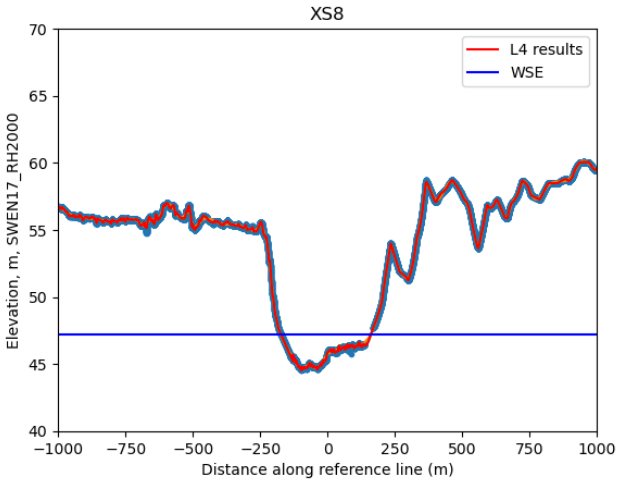


**Figure 35:** XS8

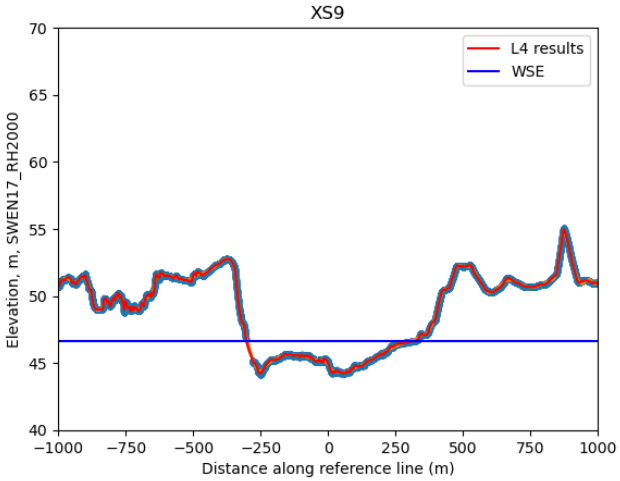


**Figure 36:** XS9

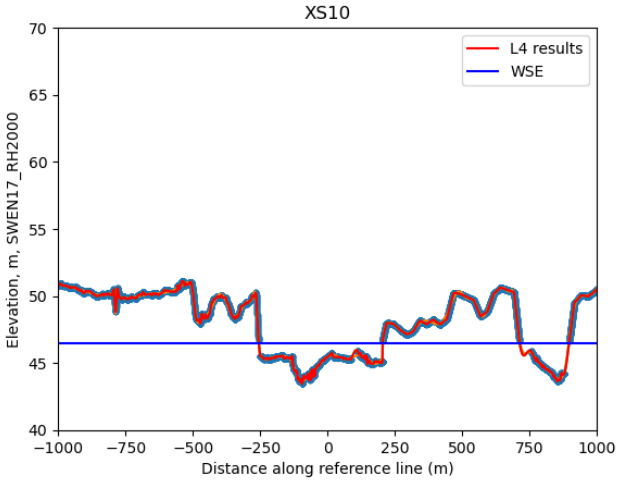


**Figure 37:** XS10

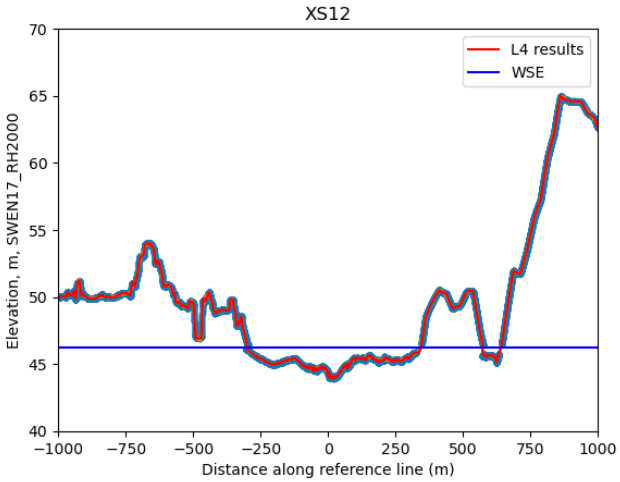


**Figure 38:** XS12

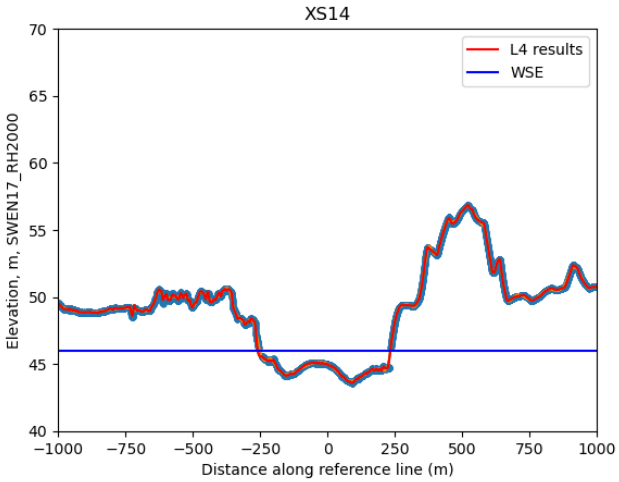


**Figure 39:** XS14

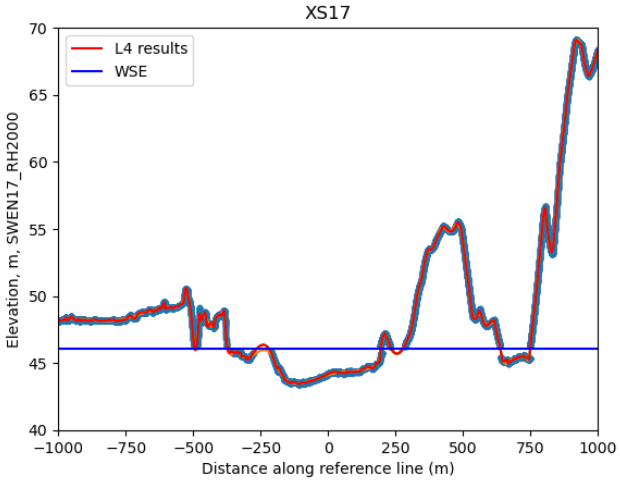


**Figure 40:** XS17

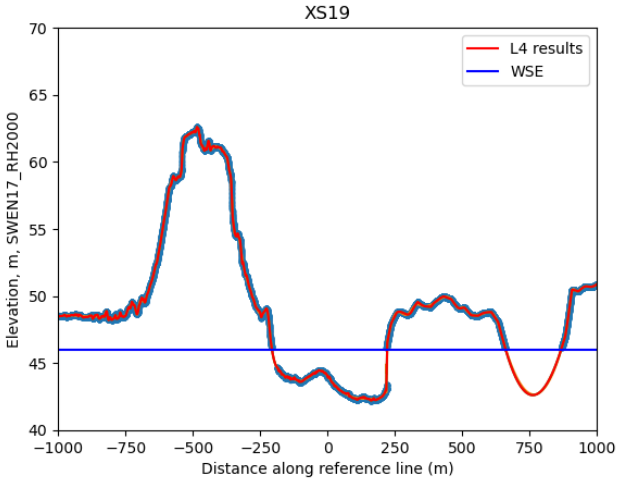


**Figure 41:** XS19

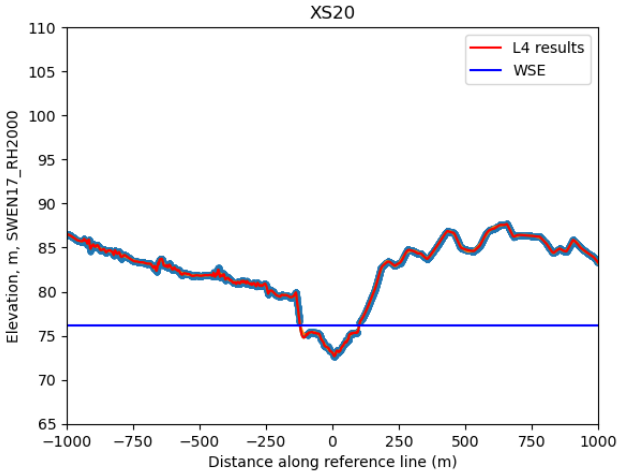


**Figure 42:** XS20

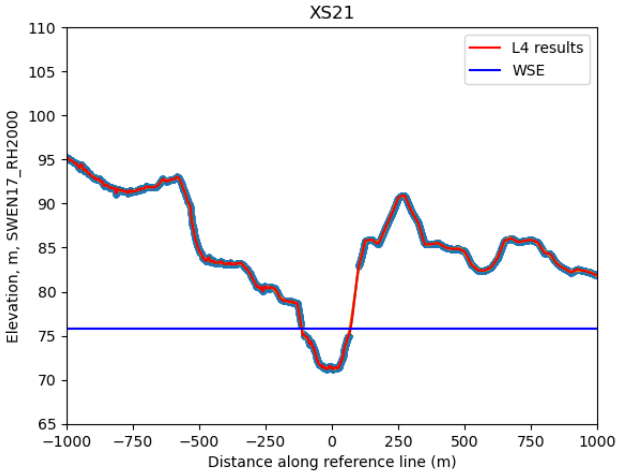


**Figure 43:** XS21

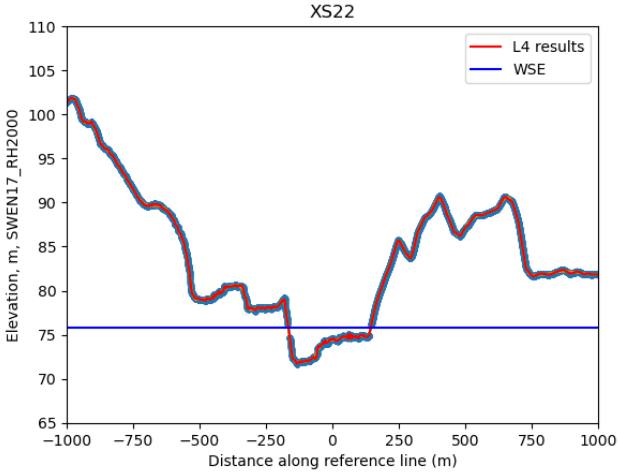


**Figure 44:** XS22

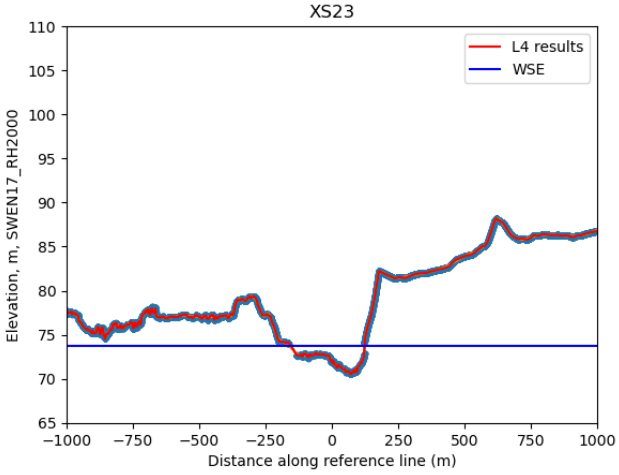


**Figure 45:** XS23

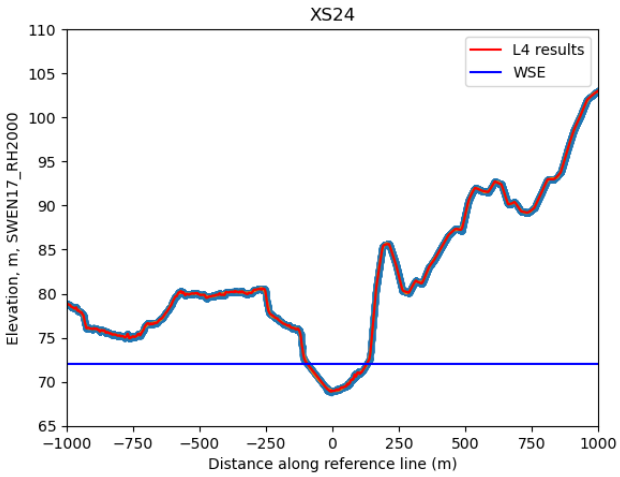


**Figure 46:** XS24

## 7.5 Rating curves

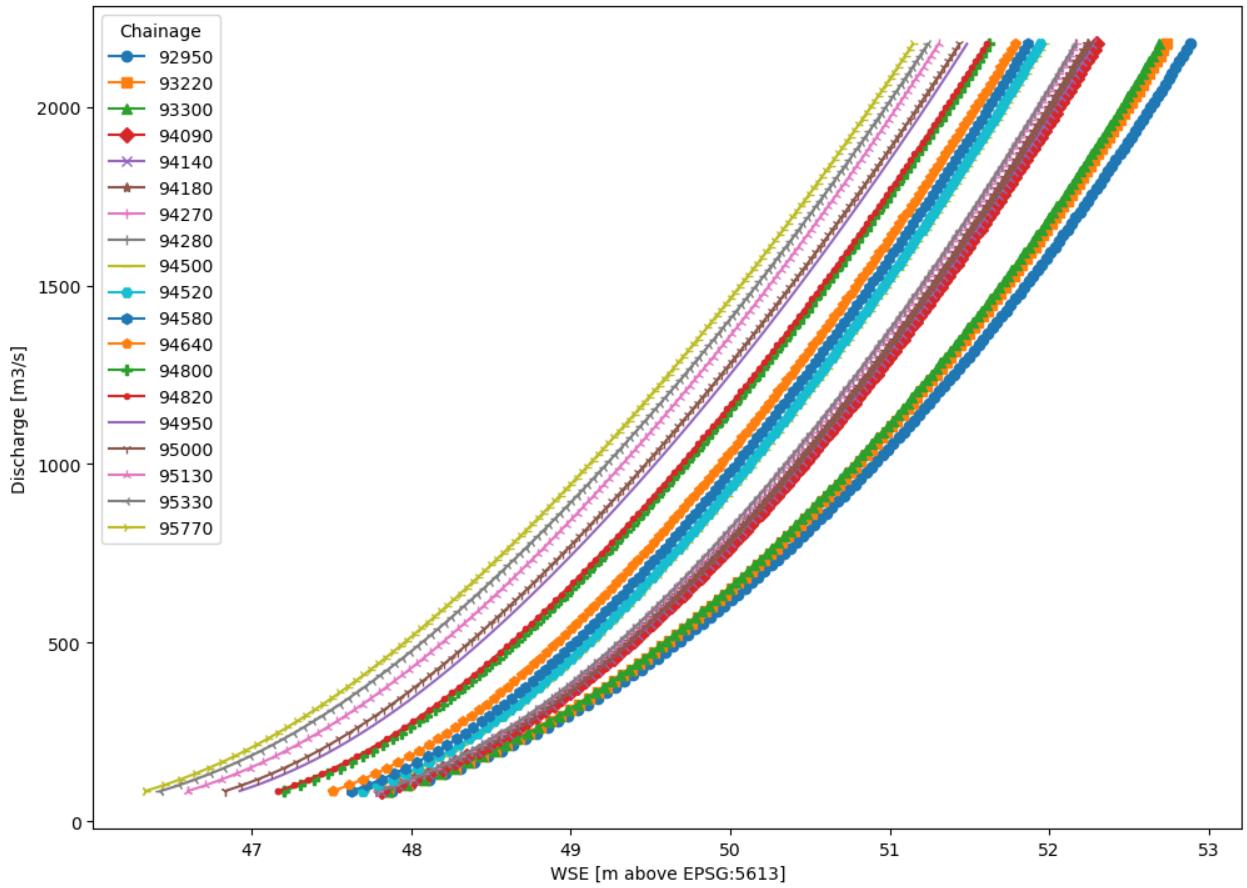


**Figure 47:** Rating curves at different chainage points in the Övertorneå virtual station made based on hydraulic model for area 1.

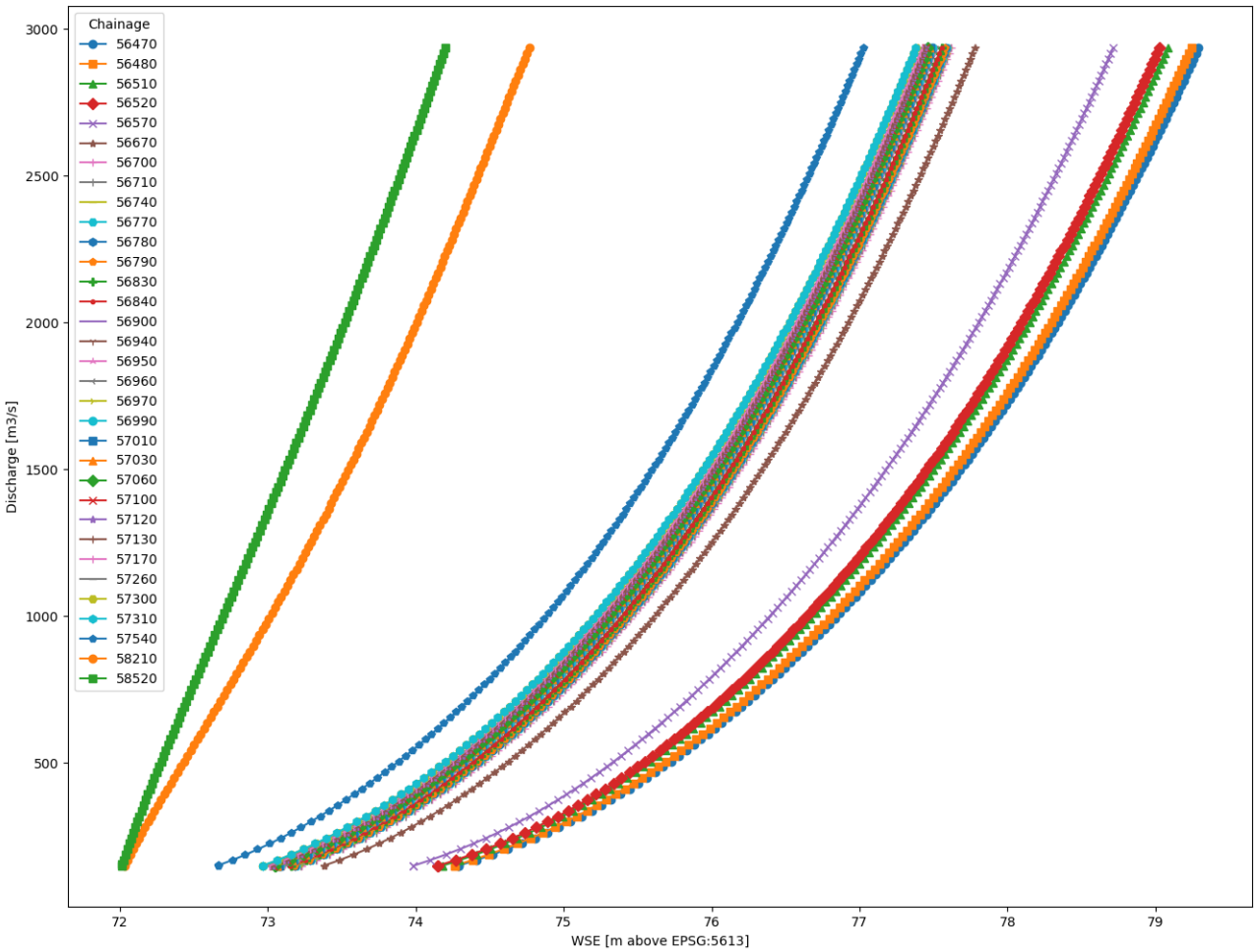


**Figure 48:** Rating curves at different chainage points in the Pello virtual station made based on hydraulic model for area 2.

## 7.6 Electric conductivity

| Date | Time | Latitude | Longitude | Water EC ($\mu\mathrm{S/cm}$) |
|---|---|---|---|---|
| 9/5/2024 | 6:30 | 66.3958728 | 23.6449338 | 37 |
| 9/5/2024 | 10:40 | 66.38013300 | 23.6824059 | 30 |
| 9/5/2024 | 13:26 | 66.38013300 | 23.6824059 | 30 |
| 9/5/2024 | 14:41 | 66.3962977 | 23.6659378 | 32 |
| 9/5/2024 | 6:43 | 66.4141775 | 23.649462 | 29 |
| 9/6/2024 | 12:02 | 66.4938604 | 23.7124135 | 33 |
| 9/6/2024 | 13:16 | 66.509178 | 23.747763 | 26 |
| 9/6/2024 | 15:25 | 66.4893503 | 23.7121751 | 28 |
| 9/6/2024 | 16:33 | 66.4769269 | 23.7130542 | 30 |
| 9/6/2024 | 17:52 | 66.4803435 | 23.7148144 | 28 |
| 9/6/2024 | 19:14 | 66.4640111 | 23.6571268 | 32 |
| 9/7/2024 | 10:25 | 66.4277232 | 23.6505 | 37 |
| 9/7/2024 | 11:40 | 66.4418893 | 23.6530763 | 30 |
| 9/7/2024 | 13:40 | 66.4847806 | 23.7191039 | 28 |
| 9/7/2024 | 14:40 | 66.4975332 | 23.7280145 | 28 |
| 9/7/2024 | 15:25 | 66.5021556 | 23.7443411 | 27 |
| 9/8/2024 | 09:48 | 66.7556606 | 23.8750388 | 33 |
| 9/8/2024 | 12:42 | 66.7856163 | 23.9095716 | 27 |
| 9/8/2024 | 14:19 | 66.7776725 | 23.9179679 | 32 |
| 9/8/2024 | 17:21 | 66.7682071 | 23.8860583 | 31 |